

The rise of van der Waals multiferroic heterostructures: Interfacial physics and devices

Yihao Zhao(赵一豪), Hongxu Duan(段虹旭), Tai Min(闵泰), and Tao Li(李桃)
Citation: Chin. Phys. B, 2026, 35 (**6**): 067501. DOI: 10.1088/1674-1056/ae3e73
http://cpb.iphy.ac.cn; http://iopscience.iop.org/cpb

What follows is a list of articles you may be interested in

Magnetoelectric topology: The rope weaving in parameter space

Ying Zhou(周颖), Ziwen Wang(王子文), Fan Wang(王凡), Haoshen Ye(叶浩燊), and Shuai Dong(董帅)
Chin. Phys. B, 2026, 35 (**2**): 027501. DOI: 10.1088/1674-1056/ae2c6b

Structural evolution-enabled $BiFeO_3$ modulated by strontium doping with enhanced dielectric, optical and superparamagnetic properties by a modified sol-gel method

Sharon V S, Veena Gopalan E, and Malini K A
Chin. Phys. B, 2023, 32 (**3**): 037504. DOI: 10.1088/1674-1056/ac785b

Computational studies on magnetism and ferroelectricity

Ke Xu(徐可), Junsheng Feng(冯俊生), and Hongjun Xiang(向红军)
Chin. Phys. B, 2022, 31 (**9**): 097505. DOI: 10.1088/1674-1056/ac7b1b

Intrinsic two-dimensional multiferroicity in $CrNCl_2$ monolayer

Wei Shen(沈威), Yuanhui Pan(潘远辉), Shengnan Shen(申胜男), Hui Li(李辉), Siyuan Nie(聂思媛), and Jie Mei(梅杰)
Chin. Phys. B, 2021, 30 (**11**): 117503. DOI: 10.1088/1674-1056/ac0787

NMR evidence of charge fluctuations in multiferroic $CuBr_2$

Rui-Qi Wang(王瑞琦), Jia-Cheng Zheng(郑家成), Tao Chen(陈涛), Peng-Shuai Wang(王朋帅), Jin-Shan Zhang(张金珊), Yi Cui(崔祎), Chong Wang(王冲), Yuan Li(李源), Sheng Xu(徐胜), Feng Yuan(袁峰), Wei-Qiang Yu(于伟强)
Chin. Phys. B, 2018, 27 (**3**): 037502. DOI: 10.1088/1674-1056/27/3/037502

TOPICAL REVIEW — Multiferroicity and multicaloric effects

The rise of van der Waals multiferroic heterostructures: Interfacial physics and devices

Yihao Zhao(赵一豪)[1], Hongxu Duan(段虹旭)[1], Tai Min(闵泰)[1,2,†], and Tao Li(李桃)[1,‡]

[1] *Center for Spintronics and Quantum Systems, State Key Laboratory for Mechanical Behavior of Materials, School of Materials Science and Engineering, Xi'an Jiaotong University, Xi'an* 710049, *China*

[2] *National Laboratory of Solid-State Microstructures and School of Materials Science and Intelligent Engineering, Nanjing University, Suzhou* 215163, *China*

(Received 1 December 2025; revised manuscript received 26 January 2026; accepted manuscript online 28 January 2026)

Van der Waals (vdW) multiferroic heterostructures, formed by stacking two-dimensional (2D) ferroelectric and magnetic materials, have emerged as a highly promising platform for next-generation electronic devices. The atomically sharp, dangling-bond-free interfaces of these heterostructures, combined with unprecedented design freedom unrestricted by lattice-matching constraints, provide an ideal playground for exploring novel magnetoelectric phenomena. This review systematically surveys the fundamental progress, challenges, and future applications in this rapidly advancing field. We begin by examining the three key interfacial magnetoelectric coupling mechanisms that have been theoretically proposed: polarization-gated interfacial charge transfer, interfacial orbital hybridization, and polarization-modulated interfacial Dzyaloshinskii–Moriya interaction (DMI). Subsequently, we bridge theory and practice by reviewing pivotal experimental demonstrations, from initial proof-of-concept work in hybrid-dimensional systems and intrinsic-mechanism explorations in low-temperature all-vdW systems to the landmark breakthrough of non-volatile electrical control of magnetism at room temperature. Building on this physical foundation, we highlight the immense potential of this field for future device applications, focusing on three promising paradigms, including ultra-low-power memory and logic, brain-inspired neuromorphic computing, and topological spintronics based on the electrical manipulation of skyrmions. Finally, we conclude by summarizing current research bottlenecks and outlining key future directions to transition this promising field from fundamental research to tangible technology.

Keywords: multiferroics, Van der Waals heterostructures, magnetoelectric coupling, two-dimensional materials, spintronics

PACS: 75.85.+t, 07.79.−v, 77.55.Nv, 68.65.−k

DOI: 10.1088/1674-1056/ae3e73 **CSTR:** 32038.14.CPB.ae3e73

1. Introduction

The exploration of advanced functional materials often begins with understanding their fundamental ordering phenomena. Central to the field of multiferroics is the concept of a ferroic order,[1,2] which refers to the spontaneous formation of a long-range ordered state of a physical quantity, including electric dipole, spin, and strain within a material in the absence of an external field. A crucial characteristic of any ferroic state is that this spontaneous order can be reversibly switched between at least two stable states by applying a corresponding external field, for instance, an electric field, a magnetic field, or mechanical stress.[3] The three main ferroic forms of ordering are ferromagnetism, ferroelectricity, and ferroelasticity, characterized by the spontaneous alignment of magnetic moments, electric polarization, and lattice strain, respectively (Fig. 1). With these definitions in place, multiferroicity can be formally defined as the phenomenon where at least two of these primary ferroic orders coexist within a single-phase material.[4,5] The coexistence of electric and magnetic orders is of particular interest for next-generation information technologies. This review will focus on magnetoelectric multiferroicity, a compelling subset of multiferroics where ferroelectric and (anti)ferromagnetic orders are simultaneously present and potentially coupled.

A true single-phase multiferroic material is one in which two or more ferroic orders coexist within a single, homogeneous crystallographic phase at the microscopic level, as opposed to a composite material formed by the physical mixture of multiple different phases (e.g., a mixture of ferroelectric and ferromagnetic nanoparticles). Based on the underlying physical origins of their ferroic orders, magnetoelectric multiferroics are generally classified into two distinct categories: type-I and type-II multiferroics.[9] Type-I multiferroicity describes materials in which ferroelectricity and magnetism typically originate from distinct ions or sublattices within the unit cell,[10] where ferroelectricity might originate from the off-center displacement of ions (e.g., in perovskite structures), while magnetism arises from superexchange interactions between transition metal ions. The primary advantage of this

†Corresponding author. E-mail: tai.min@nju.edu.cn

‡Corresponding author. E-mail: taoli66@xjtu.edu.cn

© 2026 Chinese Physical Society and IOP Publishing Ltd. All rights, including for text and data mining, AI training, and similar technologies, are reserved.

class is that the ferroic properties themselves can be quite robust, often exhibiting high ferroelectric Curie temperatures ($T_{CE} \gg 300$ K) and magnetic ordering temperatures (T_{CM}).[9] However, the limitation is that because the two orders originate from distinct subsystems, the direct magnetoelectric coupling is often limited,[11] making it difficult to achieve efficient electrical control of magnetism. In contrast, type-II multiferroicity, also known as magnetically induced multiferroicity, includes materials where ferroelectricity is directly induced by a specific, complex magnetic order that breaks spatial inversion symmetry.[12,13] In these systems, the electric and magnetic orders are intrinsically and strongly coupled by their very nature; manipulating one order parameter will inevitably have a strong effect on the other. The disadvantage, however, is that the ferroelectricity is often weak and, more critically, its existence is entirely contingent upon the magnetic order. This means that the ferroelectric state can only exist at temperatures below the magnetic ordering temperature, which for most known type-II multiferroics is typically far below room temperature.[14,15] This fundamental trade-off between strong coupling and high operating temperature has been a long-standing challenge in the field.

The classification into type-I and type-II multiferroics highlights a fundamental dilemma: achieving both strong ferroic properties and strong coupling in a single material is exceptionally difficult. The reason why high-performance single-phase multiferroics are so rare is a fundamental conflict at the atomic level, widely known as the d-orbital problem.[16] In mainstream systems such as perovskite oxides, which host many of the best-performing ferroelectrics, strong ferroelectricity typically requires the transition metal ion's d orbitals to be empty (a d^0 electronic configuration).[17,18] This emptiness facilitates hybridization with neighboring oxygen p-orbitals, which is essential for the off-center ionic displacement that generates the electric dipole moment. In stark contrast, strong magnetism (ferromagnetism or ferrimagnetism) requires the d-orbitals to be partially filled (a d^n configuration, where $n > 0$) to provide the unpaired electron spins that produce a net magnetic moment.[19,20] These two mutually exclusive requirements for d-orbital occupancy — emptiness for ferroelectricity versus partial filling for magnetism — fundamentally limit the emergence of single-phase materials simultaneously exhibiting good ferroelectric and good ferromagnetic properties. This intrinsic constraint is a primary reason the search for a room-temperature, single-phase, strong magnetoelectric multiferroic remains one of the grand challenges in materials science.

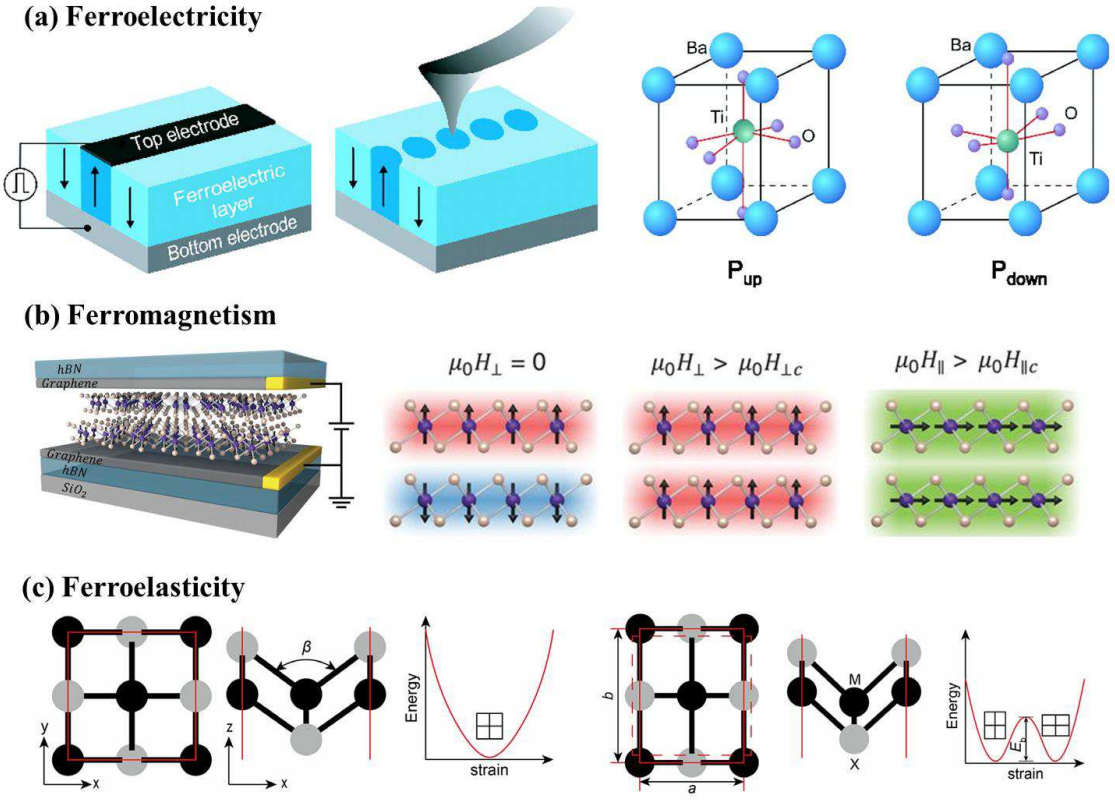


Fig. 1. Schematic of the three primary ferroic orders. Each order possesses a spontaneous long-range order parameter switchable by a conjugate external field. (a) Ferroelectricity, characterized by a spontaneous electric polarization (P) switchable by an electric field (E). The illustration shows its microscopic origin in a perovskite unit cell (e.g., $BaTiO_3$), where the off-center displacement of the central cation relative to the anions creates an electric dipole. (b) Ferromagnetism, defined by a spontaneous magnetization (M) reorientable by a magnetic field (H). The schematic depicts the parallel alignment of atomic spins in a van der Waals heterostructure. (c) Ferroelasticity, characterized by a spontaneous strain (ε) switchable by mechanical stress (σ). Panel (a) reprinted with permission from Ref. [6]. Panel (b) reprinted with permission from Ref. [7]. Panel (c) reprinted with permission from Ref. [8].

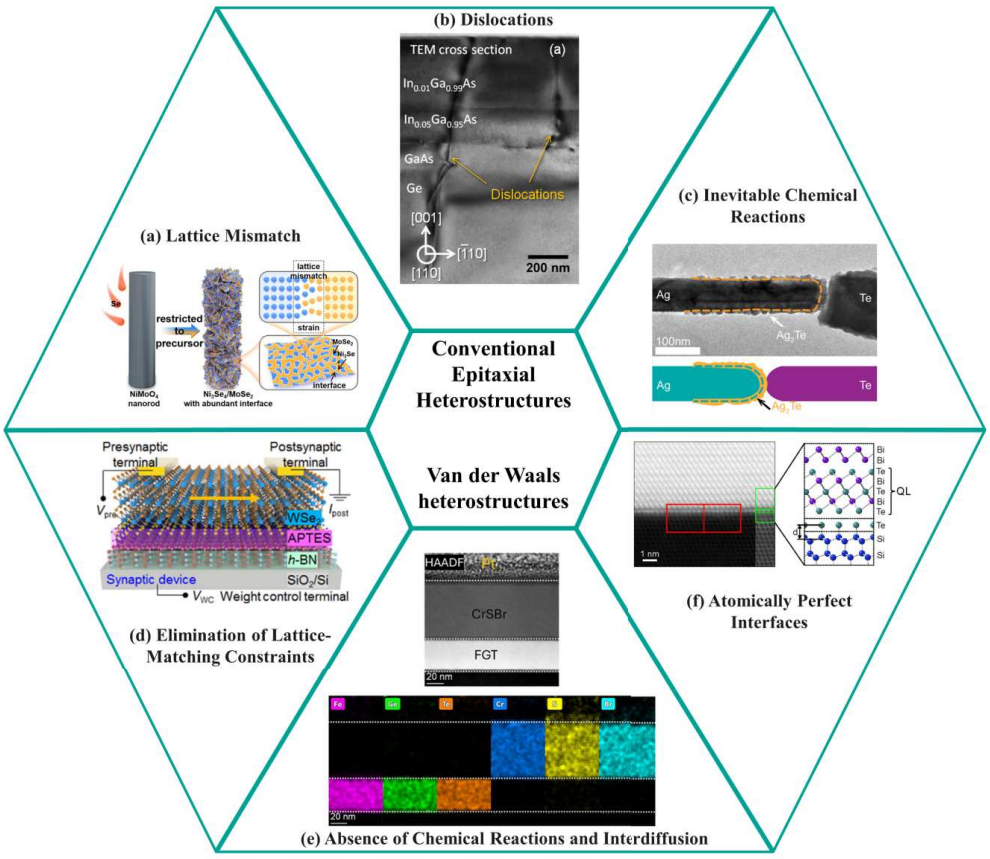


Fig. 2. A comparison between the interfacial challenges in conventional epitaxial heterostructures and the unique advantages of van der Waals heterostructures. This figure illustrates the three main challenges of conventional chemically bonded interfaces (top half) and how van der Waals interfaces (bottom half) address them. (a) Lattice mismatch: Conventional epitaxy introduces detrimental strain due to differences in lattice constants between materials. (b) Dislocations: To relieve this strain, a high density of misfit dislocations inevitably forms, compromising structural integrity. (c) Inevitable chemical reactions: Interfacial atomic diffusion and chemical reactions often create performance-degrading "dead layers". (d) Elimination of lattice–matching constraints: Stacking via van der Waals forces removes the stringent requirement of lattice matching, offering vast freedom in material combination. (e) Absence of chemical reactions and interdiffusion: The inert vdW gap effectively prevents atomic intermixing, preserving the intrinsic properties of each constituent material. (f) Atomically perfect interfaces: The absence of chemical bonds allows for the formation of atomically sharp, pristine, and dislocation-free junctions. Panel (a) reprinted with permission from Ref. [37]. Panel (b) reprinted with permission from Ref. [38]. Panel (c) reprinted with permission from Ref. [28]. Panel (d) reprinted with permission from Ref. [39]. Panel (e) reprinted with permission from Ref. [40]. Panel (f) reprinted with permission from Ref. [41].

Given the intrinsic chemical constraints that make finding ideal single-phase multiferroics so difficult, a natural and highly successful strategy has been to turn to interface engineering via heterostructures. This approach involves stacking a thin film of a high-performance ferroelectric material with a thin film of a robust ferromagnetic material, typically through methods like epitaxial growth, to form an artificial multiferroic heterostructure. The key advantage of this paradigm is functional separation by selecting the best-performing materials for each function. One can bypass the "d-orbital problem" and design a system that combines robust ferroelectricity with strong ferromagnetism. Successful examples include the work by Madon *et al.*, who synthesized epitaxial BTO-BFO/LSMO heterostructures that exhibit room-temperature ferromagnetic resonance with low damping.[21] Similarly, Prajapat *et al.* demonstrated interface-induced magnetization and exchange bias in LSMO/BFO multilayers, effectively coupling the ferroic orders.[22] Furthermore, Kumar *et al.* investigated LSMO/BFO bilayers, highlighting the critical role of controlling interfacial diffusion to maintain the functional properties of the artificial multiferroic system.[23] However, these classic epitaxial heterostructures face several challenges. The first and most significant hurdle is lattice mismatch.[24,25] The stringent requirement for compatible lattice constants between the two materials limits the materials that can be combined, reducing design freedom. The interface may also suffer from residual strain, dislocations,[26] atomic interdiffusion,[27] and unwanted chemical reactions.[28] These complex physicochemical processes create an electronically disordered region often referred to as a "dead layer".[29] This dead layer not only degrades the intrinsic performance of the individual ferroic layers but also severely weakens the pristine magnetoelectric coupling channels, thereby destroying the function of the heterojunction.

Along with the rapid development of two-dimensional van der Waals (vdW) ferroelectric and ferromagnetic materials in the past decade, researchers have turned their attention to the vdW heterostructures constructed from these 2D materials.[30] The first and most transformative advantage is the elimination of lattice matching constraints.[31,32] 2D ma-

terials are stacked via weak vdW forces, a process akin to physical adhesion rather than chemical bonding. In principle, any 2D ferroelectric can be combined with any 2D ferromagnet, regardless of their crystal structures or lattice constants, thereby expanding the freedom of materials design and opening an immense space of previously inaccessible material combinations. Secondly, this unique stacking method enables the creation of atomically flat interfaces.[33,34] The vdW interface is a physical contact, not a chemical bond, allowing the formation of pristine, atomically sharp interfaces free of dangling bonds and chemical reactions that plague epitaxial systems. This unprecedentedly clean interface provides an ideal physical platform for studying intrinsic magnetoelectric coupling driven purely by electronic interactions, without the complicating and often detrimental effects of interfacial disorder and chemical reconstruction. Finally, the inherent nature of 2D materials provides rich tunability.[35,36] The atomic thickness of the constituent layers makes their electronic and magnetic properties extremely sensitive to external stimuli. This high sensitivity, combined with the clean interface, promises a new regime of ultra-efficient modulation of magnetic properties. By designing the material components, stacking sequence, and twist angles on demand, researchers have successfully induced and tuned an exceptionally wide variety of macroscopic quantum properties, which makes this platform an ideal choice for exploring and realizing strongly coupled multiferroicity. The unique advantages of vdW heterostructures over conventional epitaxial heterostructures are shown in Fig. 2.

However, vdW heterostructures present unique challenges and disadvantages that define the current research frontiers and will be a central theme of this review. First, there is the fundamental challenge of material stability and operating temperature. Many 2D magnets (e.g., CrI_3) and some ferroelectrics are highly unstable in ambient conditions, readily degrading in air and moisture.[42] This necessitates the use of inert environment fabrication and characterization, significantly increasing experimental complexity. Furthermore, the Curie temperatures of most known 2D magnets are often far below room temperature,[43–46] which has been a fundamental material bottleneck for the development of practical applications. Second, the field faces significant fabrication challenges. The mainstream mechanical exfoliation with manual stacking technique, while capable of producing high-quality proof-of-concept devices, suffers from notoriously low yield and small sample sizes (typically on the scale of micrometers). More importantly, this process inevitably introduces interface contaminants, such as polymer residues from the transfer process or trapped air and water bubbles,[47–49] which compromise the integrity of the interface. Finally, the vdW force that enables the flexible combination of disparate materials is itself a weak interaction.[50,51] This raises a core scientific question of how to ensure the strong magnetoelectric coupling effect, which must operate across the vdW gap. Understanding, predicting, and engineering strong coupling across this weakly bonded interface is arguably the most critical scientific challenge at the current stage.

Despite these new challenges, vdW heterostructures offer an unprecedented opportunity to design a new generation of multiferroic materials on demand. Understanding their unique interfacial coupling mechanisms is the key to leveraging their advantages and overcoming their disadvantages.

2. Fundamental theories and coupling mechanisms

Van der Waals heterostructures provide an ideal platform for constructing artificial multiferroic materials. This section illustrates the fundamental principles of creating new properties by stacking 2D materials, reviews the origins of 2D ferroelectric and ferromagnetic properties, and systematically analyzes the core interfacial magnetoelectric coupling mechanisms.

2.1. 2D interface engineering: physics beyond single-phase materials

Stacking 2D materials introduces new structural degrees of freedom — including interlayer distance, stacking order, and twist angle — that give rise to emergent quantum phenomena absent in the constituent materials.[52–54] This approach extends beyond simple composites, allowing for the creation of new physical states through precise interface design.

Several mechanisms are central to these interface-driven principles. The first is the proximity effect.[55–57] When a 2D material, such as graphene, is stacked with another material like a TMD or a superconductor, the properties of the latter can be induced in the former. Through wavefunction overlap at the interface, features such as strong spin–orbit coupling or superconducting order are transferred, modifying the material's intrinsic properties.

Interface engineering also leads to the formation of moiré superlattices.[58–60] When two 2D materials with similar lattice constants or with a slight twist angle are stacked, a long-period moiré pattern is formed. This moiré pattern creates a periodic potential modulation that significantly modifies the electronic band structure of the system, leading to the formation of flat bands and topological bands.[61,62] Therefore, moiré systems are now an ideal platform for studying strongly correlated electronic states, such as correlated insulators and unconventional superconductors.

Finally, interactions at the interface can drive interfacial reconstruction and the emergence of new phases. The associated symmetry breaking gives rise to emergent physical states that do not exist in the individual layers, such as sliding ferroelectricity and interfacial excitons.[63,64] For instance, a recent study by Wang *et al.* demonstrated the electric control of

magneto-excitons in the van der Waals antiferromagnet $NiPS_3$, offering a new avenue for magneto-optical devices.[64]

The principles of interface engineering described above offer a physical basis for constructing 2D multiferroics. Stacking 2D materials introduces new degrees of freedom, particularly the twist angle, which can reconstruct the electronic structure via the moiré potential. This reconstruction suppresses the kinetic energy of electrons and leads to flat bands. As a result, interactions that are typically subtle — such as electron correlations and proximity effects — become dominant. 2D multiferroic heterostructures utilize this mechanism to amplify electron interactions. This approach induces strong magnetoelectric coupling in systems that might otherwise be non-magnetic or weakly coupled.

2.2. Origins of ferroelectricity and magnetism in 2D systems

Designing multiferroics via interface engineering requires understanding how 2D ferroelectric and ferromagnetic orders stabilize in the 2D limit. This section reviews the intrinsic properties of these constituent materials to provide context for their interfacial interactions.

2.2.1. Primary mechanisms of 2D ferroelectricity

As shown in Fig. 3(a), the physical mechanisms for 2D ferroelectricity can be divided into two main classes. The first is intralayer ionic displacement, the most conventional mechanism, where a spontaneous relative displacement between cations and anions occurs within a single atomic layer, creating a net electric dipole moment. This can manifest as out-of-plane polarization (e.g., in α-In_2Se_3)[65–67] or in-plane polarization (e.g., in group-IV monochalcogenides).[68–70] The second class is sliding ferroelectricity. Unlike internal ionic shifts, this form of ferroelectricity originates from the lateral translation of one atomic layer relative to another, where the sliding motion breaks the inversion symmetry of the stacking configuration to induce an out-of-plane polarization, as exemplified by bilayer WTe_2.[63,71] A related variant is topologically driven ferroelectricity, in which intrinsic dipoles arise from sublattice asymmetry in certain special lattices.[72,73] Furthermore, other emerging mechanisms also exist, such as reconstructive ferroelectricity, and notably, purely electronic ferroelectricity was observed recently, which is driven by interlayer charge reconstruction rather than ionic displacement. This diversity of parallel physical origins provides a rich platform for the discovery of novel 2D ferroelectrics.

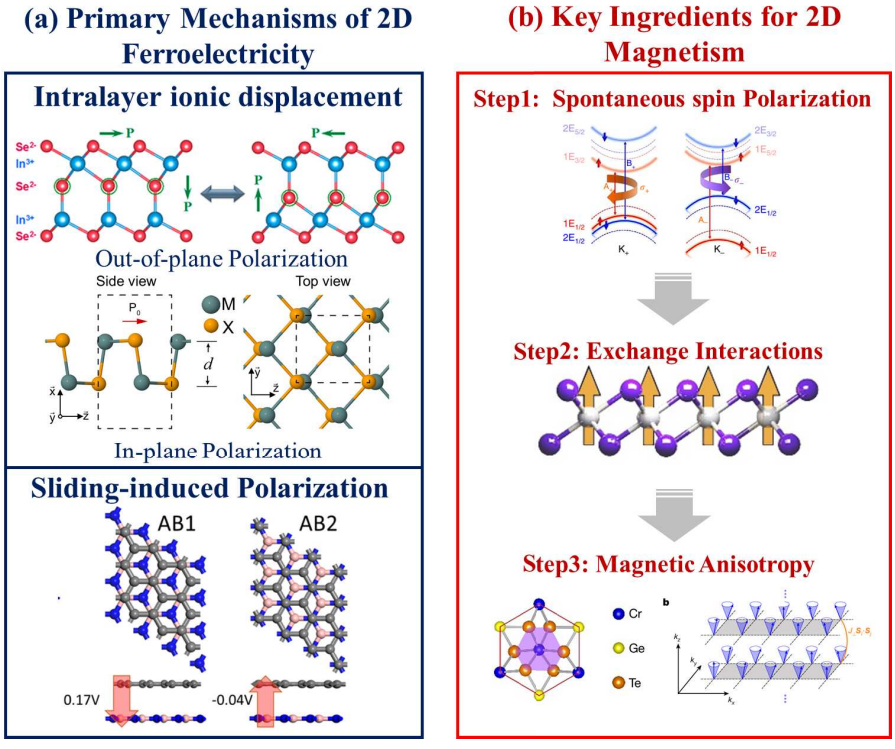


Fig. 3. Physical origins of 2D ferroelectricity and magnetism. This figure contrasts the multiple parallel mechanisms for 2D ferroelectricity with the progressive key ingredients required for stable 2D magnetism. (a) Primary mechanisms of 2D ferroelectricity: Two primary classes of physical mechanisms are illustrated. The first class is intralayer ionic displacement, where a relative shift of cations and anions within a layer generates a spontaneous polarization. This mechanism can manifest as either out-of-plane polarization (top, e.g., in α-In_2Se_3) or in-plane polarization (middle, e.g., in SnTe). The second class is interlayer sliding (bottom), where a relative lateral translation between atomic layers induces a polarization across the van der Waals interface. (b) Key ingredients for stabilizing 2D magnetism: Three sequential steps required for stabilizing long-range magnetic orders are illustrated. Step 1: The material must possess spontaneous spin polarization from unpaired electrons to provide local magnetic moments. Step 2: Exchange interactions must be present to couple these local moments into a collective magnetic order. Step 3: A finite magnetic anisotropy is essential to open an energy gap that suppresses thermal fluctuations, thereby stabilizing the 2D magnetic order at finite temperatures. Panel (a) reprinted with permission from Refs. [66,68,71]. Panel (b) reprinted with permission from Refs. [76,79,80].

2.2.2. Primary mechanisms of 2D magnetism

As shown in Fig. 3(b), similar to ferroelectricity, stabilizing long-range magnetic order in the 2D limit also faces fundamental physical challenges. According to the Mermin–Wagner theorem,[74] in a 2D system possessing continuous spin rotational symmetry, thermal fluctuations preclude the formation of long-range order at any non-zero temperature. Stabilizing long-range magnetic order in the 2D limit therefore requires satisfying a set of strict conditions that overcome these thermal fluctuations. First, the presence of local magnetic moments,[75,76] which typically arise from unpaired electrons in d or f orbitals, serves as the fundamental material basis for magnetism. Building upon this, exchange interactions are required as the driving force to couple these local moments into a collectively ordered state, be it ferromagnetic (FM) or antiferromagnetic (AFM).[77,78] Finally, there must be a sufficiently strong magnetic anisotropy.[79,80] This provides the stabilizing factor by breaking the continuous rotational symmetry of spins, creating an energy barrier (an easy axis) that suppresses long-wavelength thermal fluctuations and allows long-range magnetic order to persist at finite temperatures. These three steps are sequential, and each is indispensable; together they form the complete physical picture for the existence of stable 2D magnetism.

While the physical mechanisms discussed above enable the stabilization of independent 2D ferroelectric and magnetic orders, intrinsic single-phase 2D multiferroics remain scarce and typically suffer from low critical temperatures or limited tunability. To overcome these inherent material constraints, a more robust approach involves integrating these distinct functional layers via van der Waals stacking. This strategy bypasses the chemical exclusions that restrict single-phase compounds, enabling the construction of artificial multiferroic heterostructures where the operating conditions and magnetoelectric performance can be engineered directly through interface design.

The core advantage of this strategy lies in its immense flexibility, but it also introduces a new and more fundamental scientific question: when a ferroelectric layer and a magnetic layer are brought into atomic proximity, can they generate an effective interaction? What is the physical nature of this interaction across a van der Waals gap, which leads to the magnetoelectric coupling? In the following section, we will focus on the key interfacial magnetoelectric coupling mechanisms that have been theoretically proposed.

2.3. Interfacial magnetoelectric coupling mechanisms in vdW heterostructures

In contrast to bulk heterostructures mediated by chemical bonds and strain, coupling in van der Waals systems is a purely interfacial phenomenon. Theoretical studies indicate that this coupling is not dominated by a single mechanism but is rather the result of the synergistic action of multiple physical effects. The primary and most long-range of these is the electrostatic modification of the interface.

2.3.1. Polarization-gated interfacial charge transfer

A primary and potent coupling mechanism in van der Waals (vdW) multiferroic heterostructures arises from the non-volatile gating of interfacial charge transfer by the ferroelectric polarization, which is shown in Fig. 4. The physical origin of this mechanism lies in the built-in electric field intrinsic to a ferroelectric material, a consequence of ionic displacement. This field breaks spatial inversion symmetry and leads to disparate work functions or electrostatic potentials on its opposite surfaces. Consequently, when a heterostructure is formed, switching the ferroelectric polarization via an external field fundamentally and non-volatilely reconfigures the overall electrostatic potential profile, thereby inducing a dramatic and reversible reconstruction of the band alignment between the constituent layers.

This polarization-driven band reconstruction acts as a critical switch for controlling interfacial charge transfer. First-principles calculations explicitly demonstrate this effect, showing that the type of band alignment is highly sensitive to the ferroelectric polarization state. For instance, in the bilayer CrI_3/Sc_2CO_2 heterostructure,[81,82] one polarization state results in a type-II alignment where the band gaps are staggered, suppressing effective charge transfer. Upon polarization reversal, however, the band structure transitions to a type-III alignment. In this configuration, the conduction band minimum (CBM) of the magnetic CrI_3 lies below the valence band maximum (VBM) of the ferroelectric Sc_2CO_2, creating a favorable condition for spontaneous electron transfer. This switching of the alignment type effectively opens or closes the channel for interlayer charge flow.

The change in band alignment subsequently drives a directional interfacial charge transfer. Quantitative methods like Bader charge analysis confirm that upon polarization switching, both the magnitude and even the direction of charge transfer across the vdW interface are deterministically altered. For example, in the CrI_3–$AgBiP_2Se_6$ heterostructure, reversing the polarization nearly doubles the amount of electron charge transferred to the CrI_3 layer, while in the $Cr_2Ge_2Te_6$–In_2Se_3 system,[83] the direction of transfer itself is inverted. This precisely controlled injection or withdrawal of carriers, governed by the ferroelectric state, constitutes a reversible and non-volatile form of electrostatic doping into the adjacent magnetic layer.

The ultimate consequence of this controlled electrostatic doping is the effective modulation of the magnetic ground state, with two key physical manifestations. The first is the semiconductor-to-half-metal transition, which depends critically on the specific band alignment of the heterostructure.

For a ferromagnetic semiconductor like monolayer CrI_3, provided the band offsets are favorable, electrons injected from the ferroelectric layer (e.g., P↓-Sc_2CO_2) can populate its spin-polarized conduction band, transforming it into a half-metal — an effect that vanishes upon polarization reversal. The second critical effect is the ability to switch the interlayer magnetic coupling. For layered magnets with weak interlayer interactions, such as bilayer CrI_3 with its native antiferromagnetic (AFM) ground state, the magnetic order is highly susceptible to carrier density. Theoretical studies have identified electron doping as the main driving force for stabilizing the interlayer ferromagnetic (FM) state. Therefore, polarization-gated electron transfer can directly toggle the interlayer magnetic order between the AFM and FM states non-volatilely.

The physical sequence linking ferroelectric polarization, band reconstruction, and charge transfer establishes a robust mechanism for modulating the magnetic state. This approach provides a general strategy for achieving non-volatile, all-electrical control of 2D magnetism.

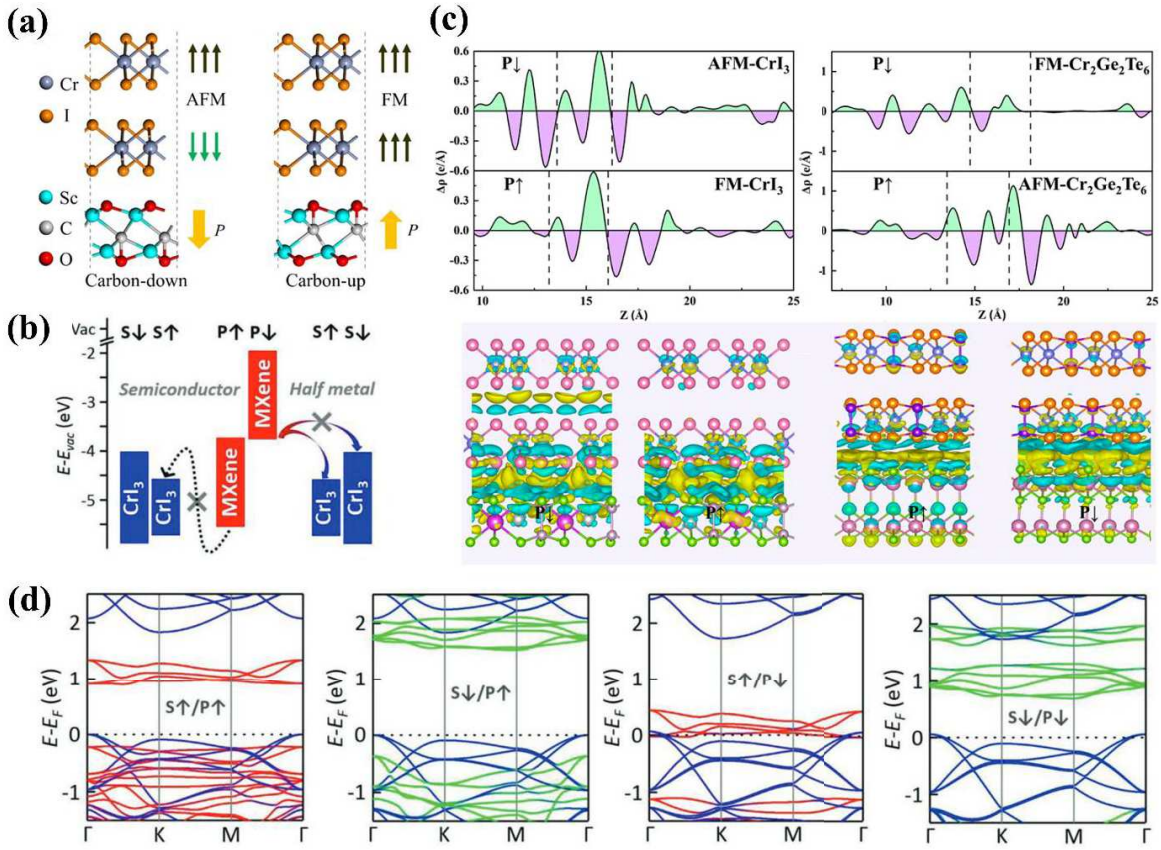


Fig. 4. Mechanism of polarization-gated interfacial charge transfer coupling. This figure systematically illustrates the physical chain for non-volatilely modulating the properties of a magnetic layer by switching the polarization of an adjacent ferroelectric layer. (a) Schematic illustration of the macroscopic phenomenon in a vdW heterostructure (e.g., bilayer CrI_3/Sc_2CO_2), showing that ferroelectric polarization reversal can toggle the interlayer magnetic coupling of bilayer CrI_3 between the antiferromagnetic (AFM) and ferromagnetic (FM) states. (b) The electronic origin of the coupling. The band alignment diagram indicates that one polarization state (P↓) reconstructs the bands into a type-III alignment, providing the driving force for charge transfer. (c) The core mechanism of the coupling. The plane-averaged differential charge density plot clearly reveals the charge redistribution, with electron depletion ($\Delta\rho < 0$) in the ferroelectric layer (e.g., $AgBiP_2Se_6$) and a corresponding electron accumulation ($\Delta\rho > 0$) in the magnetic layer (e.g., CrI_3), providing direct and quantitative evidence of interfacial charge transfer. (d) The ultimate physical consequence of the charge transfer. The calculated band structures demonstrate that the charge injection (under P↓ state) can induce a semiconductor-to-half-metal transition in the magnetic CrI_3 layer. Panel (a) reprinted with permission from Ref. [82]. Panels (b) and (d) reprinted with permission from Ref. [81]. Panel (c) reprinted with permission from Ref. [83].

2.3.2. Interfacial orbital hybridization and modulation of magnetocrystalline anisotropy

Beyond the long-range electrostatic mechanism of charge transfer, magnetoelectric coupling in vdW heterostructures can also be realized through another mechanism rooted in atomic-scale interactions. This pathway relies on directly modulating a fundamental magnetic property: the magnetocrystalline anisotropy energy (MAE), which determines the stable orientation of magnetization. Physically, the structural distortions accompanying ferroelectric switching modify the interlayer overlap of orbital wavefunctions. This variation in interfacial hybridization subsequently alters, or even reverses the sign of, the MAE in the magnetic layer, as shown in Fig. 5.

The process begins with ionic displacement within the ferroelectric layer. When the polarization of a ferroelectric material like In_2Se_3 is switched, its ions (particularly the surface Se atoms) undergo picometer-scale cooperative displacements. Although the vdW interaction is weak, this structural

modification is sufficient to change the equilibrium interlayer distance to the adjacent magnetic layer (e.g., $Cr_2Ge_2Te_6$). For example, in the $Cr_2Ge_2Te_6/In_2Se_3$ system, the equilibrium interlayer distances for the upward (P↑) and downward (P↓) polarization states of In_2Se_3 are demonstrably different (3.20 Å and 3.14 Å, respectively).

This change in interlayer spacing directly affects the strength of orbital hybridization at the interface. Specifically, the extent of wavefunction overlap between the d-orbitals of the transition metal in the magnetic layer (e.g., Cr) and the p-orbitals of the surface anions in the ferroelectric layer (e.g., Se) is highly sensitive to this distance. A reduction in interlayer distance upon polarization switching leads to an enhanced interfacial p–d orbital hybridization. This enhanced hybridization, in turn, strongly perturbs the electronic structure of the magnetic layer, particularly its spin-resolved and orbital-decomposed band structure. Calculations for the $Cr_2Ge_2Te_6/In_2Se_3$ system reveal that the downward polarization of In_2Se_3 promotes a stronger hybridization between its conduction band and that of $Cr_2Ge_2Te_6$, significantly altering the occupation of specific Cr d-orbitals (e.g., those with $|m_z| = 1$), as shown in Fig. 5(d).[84]

Ultimately, these modifications to the electronic structure alter the MAE. According to perturbation theory, the MAE originates from the spin–orbit coupling (SOC) between occupied and unoccupied d-orbital states. The polarization-modulated interfacial hybridization changes the energy and occupation of specific d-orbitals, thereby changing the competitive balance between different orbital transitions (e.g., spin-conserving versus spin-flipping) that are responsible for the sign and magnitude of the MAE. In the $Cr_2Ge_2Te_6/In_2Se_3$ heterostructure,[84,85] first-principles calculations explicitly show that switching the In_2Se_3 polarization from up to down causes the magnetic ground state of $Cr_2Ge_2Te_6$ to change from easy-plane anisotropy to easy-axis anisotropy.

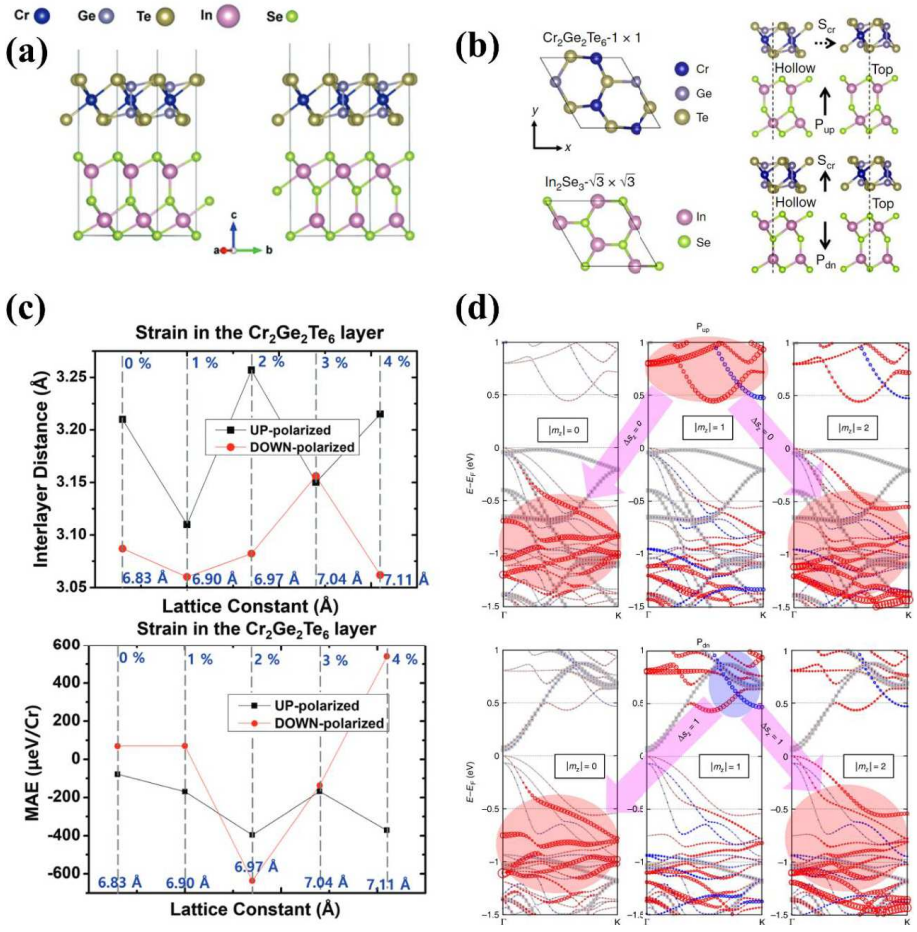


Fig. 5. Mechanism of MAE modulation driven by interfacial orbital hybridization. This figure illustrates the physical process by which ferroelectric polarization reversal alters interfacial atomic interactions to modulate the MAE. (a) Side views of the $Cr_2Ge_2Te_6/In_2Se_3$ heterostructure in its two different polarization states, showing the displacement of interfacial atoms upon polarization switching. (b) Top views and stacking configuration of the heterostructure. (c) Quantitative impact of the polarization state on interfacial structure and magnetic anisotropy. The top panel shows that the interlayer distance for the down-polarized state is systematically smaller than that of the up-polarized state, providing the structural basis for enhanced orbital hybridization. The bottom panel shows the evolution of MAE with polarization and strain: the MAE for the up-polarized state is consistently negative (easy-plane), whereas for the down-polarized state it becomes positive (easy-axis) at specific strains, resulting in a sign reversal of the MAE. (d) The electronic origin of the MAE switching. A comparison between the top (P_{up}) and bottom (P_{down}) sets of spin- and orbital-decomposed band structures reveals that the down-polarized state enhances interlayer orbital hybridization, altering the relative strength of the critical orbital transitions that determine the sign of the MAE and ultimately driving the transition from easy-plane to easy-axis anisotropy. Panels (a)–(c) reprinted with permission from Ref. [85]. Panel (d) reprinted with permission from Ref. [84].

The physical implication of modulating the MAE is profound. The presence of an easy-axis anisotropy is crucial for opening a spin-wave excitation gap, which stabilizes 2D ferromagnetism. Therefore, electrically switching the magnetic anisotropy from easy-plane to easy-axis provides a nonvolatile pathway to toggle the long-range ferromagnetic order between an "off" state and an "on" state at finite temperatures, offering a novel paradigm for magnetic memory and logic devices.

2.3.3. Polarization-modulated interfacial Dzyaloshinskii–Moriya interaction

In addition to modulating carrier concentration and magnetocrystalline anisotropy, ferroelectric polarization provides another pathway to directly control magnetic chirality by modulating the interfacial Dzyaloshinskii–Moriya interaction (DMI),[86–88] which is shown in Fig. 6. The DMI is an antisymmetric exchange interaction of the form $D \cdot (S_i \times S_j)$, whose existence requires the lack of space-inversion symmetry. In vdW heterostructures, the interface between the magnetic and ferroelectric layers breaks this symmetry, allowing for a nonzero interfacial DMI. The switchable polarization of the ferroelectric layer, which corresponds to ionic displacements, further modifies the manner of this symmetry breaking, thereby providing a physical basis for electrically controlling the DMI vector's strength and even its direction.[87,88]

First-principles calculations have systematically demonstrated the effective control of interfacial DMI by ferroelectric polarization. Studies show that the magnitude of the DMI is highly sensitive to the polarization state. In a simple bilayer heterostructure, such as Fe_3GeTe_2/In_2Se_3, reversing the polarization of the In_2Se_3 layer can induce a substantial change in the magnitude of the DMI. This "on/off" control of the DMI strength directly governs the stability of chiral magnetic textures. Since DMI is the crucial interaction for stabilizing magnetic skyrmions, modulating its magnitude via ferroelectric polarization enables the non-volatile "creation" and "annihilation" of these topological objects.[86,88]

A full reversal of the DMI vector's direction can be achieved in more symmetric sandwich structures, such as $In_2Se_3/CrI_3/In_2Se_3$ or $In_2Se_3/Fe_3GeTe_2/In_2Se_3$. In such structures, the simultaneous switching of the polarizations in the top and bottom ferroelectric layers is equivalent to a symmetry operation that leads to a complete sign reversal of the DMI vector, from D to $-D$.[87,88] A reversal of the DMI sign corresponds to a reversal of the system's magnetic chirality. For a skyrmion, this translates directly into the reversal of its chirality, meaning its internal spin-whirling direction is inverted.[88]

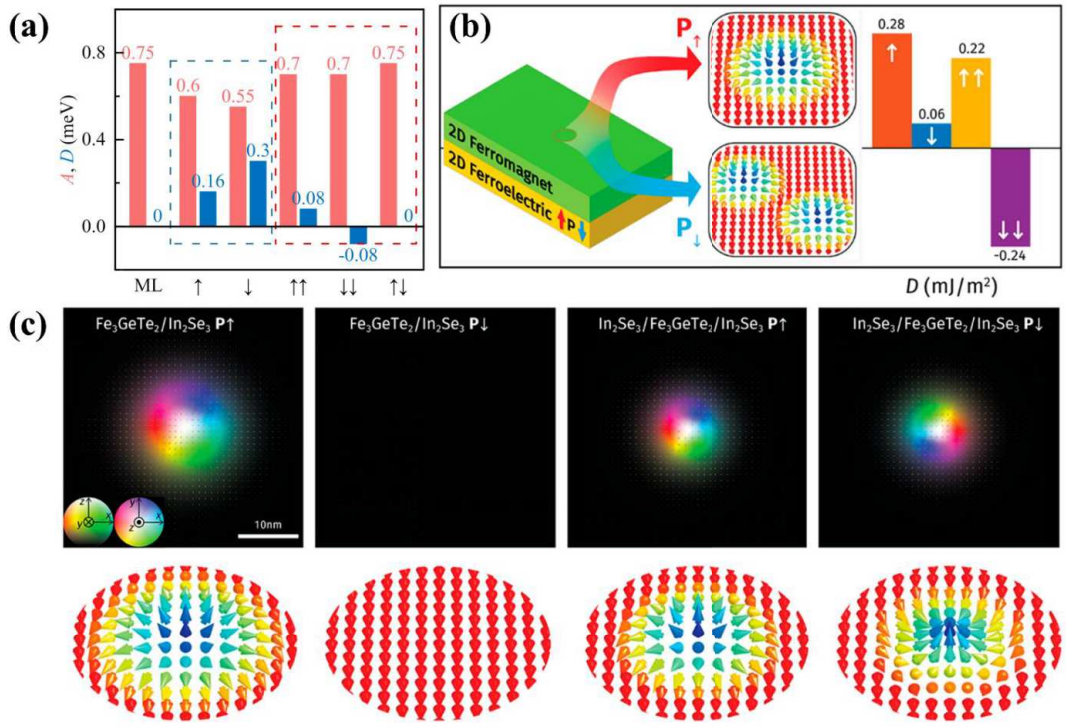


Fig. 6. Ferroelectric polarization control of interfacial DMI and its static consequences on skyrmions. This figure illustrates how ferroelectric polarization acts as a tuning knob to control the existence and properties of magnetic skyrmions by modulating the interfacial DMI. (a) First-principles calculations demonstrating the control of the DMI sign by ferroelectric polarization in a sandwich heterostructure. The sign of the DMI is fully reversed when the polarizations of the top and bottom ferroelectric layers are switched simultaneously (↑↑ vs. ↓↓). (b) Modulation of the DMI magnitude by ferroelectric polarization in a bilayer heterostructure. The schematic and the corresponding calculated values (bar chart) show that reversing the polarization can significantly alter the DMI magnitude, thereby affecting skyrmion stability. (c) Physical consequences of DMI modulation. The top panels demonstrate the reversible "creation" and "annihilation" of a skyrmion in a bilayer structure, achieved by switching the DMI magnitude via polarization reversal (P↑ vs. P↓). The bottom panels show the deterministic switching of a skyrmion's chirality in a sandwich structure, driven by the reversal of the DMI sign via synchronous polarization switching. Panel (a) reprinted with permission from Ref. [87]. Panels (b) and (c) reprinted with permission from Ref. [88].

The dynamic control of DMI also gives rise to novel physical phenomena. Theoretical work has proposed that the rapid reversal of the DMI vector via ferroelectric switching can pump an effective torque on magnetic domain walls, which has been termed the DMI torque. This torque can drive the motion of domain walls without the need for an applied electric current or magnetic field. Such a purely electric-field-driven, low-energy-consumption domain wall motion presents a highly attractive scheme for novel domain-wall-based memory devices.

In summary, the mechanism of modulating interfacial DMI via polarization enables not only static control over the existence and chirality of topological spin structures like skyrmions but also dynamic manipulation of domain walls.[86–88] This provides a physical foundation for all-electrical control of topological magnetic information carriers, highlighting a core advantage of 2D multiferroic heterostructures for future low-power, high-density spintronic applications.

2.3.4. Synergy of mechanisms

In real material systems, the three mechanisms described above are not completely independent but often act synergistically to determine the final observed magnetoelectric coupling strength and characteristics. For instance, charge transfer is almost always accompanied by a macroscopic shift in the band structure, while atomic-scale structural distortions can also influence the local charge distribution and band bending.

However, in different systems, one or two dominant mechanisms often prevail.[81,82,89] For example, in a heterostructure composed of a magnetic semiconductor, the charge transfer mechanism is likely to be most effective due to the low carrier density and high sensitivity to electrostatic doping. Conversely, in a heterostructure with a magnetic metal, the strong screening effect from the metal's free carriers will significantly weaken the macroscopic electrostatic doping effect. In such cases, the orbital hybridization and band alignment modulation mechanisms, which do not rely on charge transfer, may play a more important role.

Identifying the dominant coupling mechanism in a specific system remains a primary objective for theoretical research and is essential for device optimization. Two-dimensional van der Waals multiferroic heterostructures enable magnetoelectric coupling through the combined action of long-range electrostatic fields and short-range orbital interactions. This dual capability distinguishes them from conventional materials and underpins their potential for realizing novel physical states.

While the sections above detail the underlying physics, the experimental realization of these mechanisms is often dictated by engineering realities. To bridge the gap between theoretical prediction and device fabrication, we summarize the engineering feasibility of these coupling modes in Table 1.

Table 1. Toolbox for engineering vdW multiferroic heterostructures.

Device constraint/factor	Polarization-gated charge transfer	Interfacial orbital hybridization (MAE)	Polarization-modulated DMI
Physical origin	Long-range electrostatic field (electrostatic doping)	Short-range electronic wavefunction overlap	Symmetry breaking at the interface (antisymmetric exchange)
Screening/depolarization	(i) Highly sensitive. (ii) Requires low carrier density (magnetic semiconductors) to avoid screening of the FE field. (iii) Ineffective in metals due to short screening lengths.	(i) Robust. (ii) Operates effectively in both metals and semiconductors as it relies on local atomic bonding rather than long-range fields.	(i) Robust. (ii) Often enhanced in metallic systems with strong spin–orbit coupling (SOC).
Interface cleanliness	Moderate tolerance: Can persist through ultrathin dielectric layers (tunneling/field effect), provided the depolarization field is managed.	Zero tolerance: Requires direct, atomically sharp contact. Any interlayer (even monolayer hBN) or contaminant (dead layer) disrupts the crucial p–d orbital hybridization.	High sensitivity: Requires direct contact to break inversion symmetry and induce DMI. Interfacial disorder can randomize the DMI vector.
Domain structure	Global modulation: The magnetic state typically follows the average polarization gating; susceptible to leakage at domain walls.	Local pinning: Ferroelectric domains can locally pin magnetic domains or domain walls via strain or hybridization, affecting coercivity.	Chirality imprinting: ferroelectric domains can locally define magnetic chirality (skyrmion vs. trivial bubble) or create domain wall tracks.
Suggested material pairings	FE/Magnetic semiconductor where doping drives phase transitions	FE/Magnetic metal or semiconductor with distinct orbital symmetries	FE/Heavy metallic ferromagnet to maximize SOC and DMI strength

3. Synthesis and characterization

Theoretical models and first-principles calculations have established a framework for understanding interfacial magnetoelectric coupling in 2D van der Waals heterostructures. Validating these predictions requires translating atomic-scale concepts into functional physical devices. This transition demands advanced experimental techniques for both material fabrication and property characterization.

This section focuses on the experimental methods used to construct and investigate 2D van der Waals multiferroic heterostructures. We first review the primary technical routes for sample fabrication, distinguishing between mechanical assembly and large-area growth techniques. Subsequently, we out-

line the probing techniques required to characterize the structural, ferroelectric, and magnetic properties. These methodologies provide the basis for evaluating the experimental results discussed in later sections.

3.1. Synthesis of 2D materials and vdW heterostructures

As shown in Fig. 7, realizing theoretical predictions in experimental devices relies on obtaining high-quality materials and achieving precise heterostructure construction. In 2D multiferroics, the fabrication process governs not only the intrinsic properties of the layers but also the observability of weak interfacial magnetoelectric coupling. Fabrication techniques generally follow two primary routes: a top-down approach based on mechanical exfoliation and stacking, and a bottom-up approach focused on large-area growth.

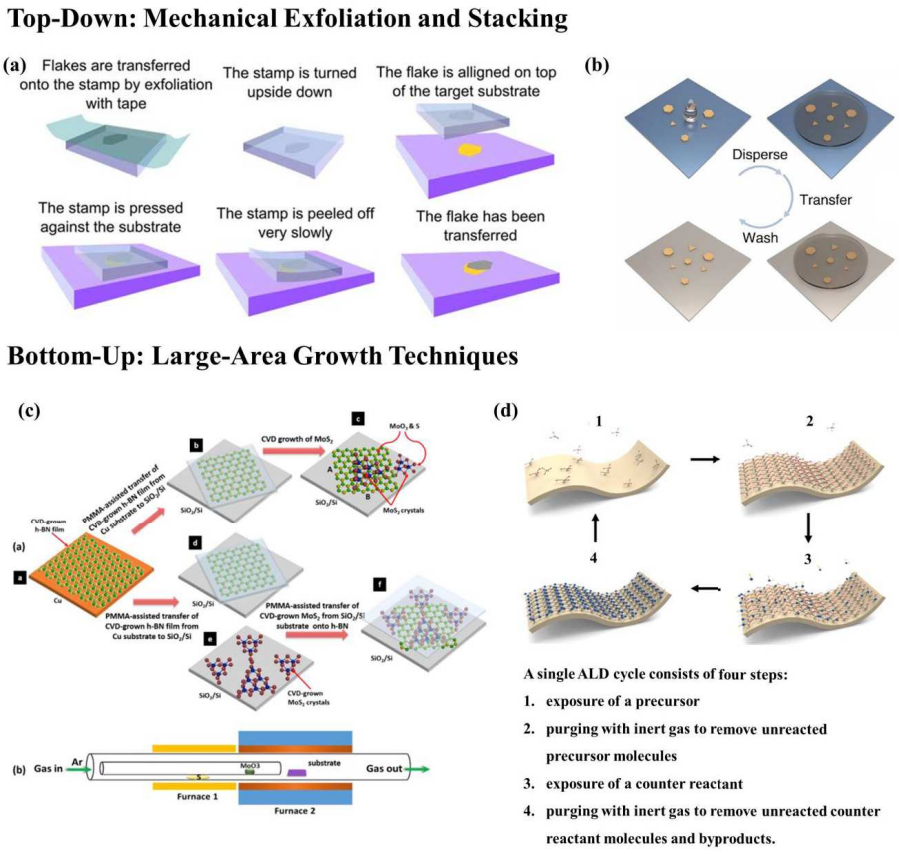


Fig. 7. Fabrication techniques for van der Waals (vdW) heterostructures. (a) and (b) Top-down mechanical assembly. (a) Mechanical exfoliation of atomically thin flakes from bulk crystals. (b) Deterministic layer-by-layer stacking using a viscoelastic stamp. Although yielding the highest crystalline quality, this method is limited by low throughput, micrometer-scale sample sizes, and potential interfacial contamination. (c) and (d) Bottom-up large-area growth. (c) Chemical vapor deposition (CVD), where gaseous precursors react at high temperatures to synthesize wafer-scale 2D films directly on substrates. (d) Atomic layer deposition (ALD), which utilizes sequential, self-limiting surface reactions to deposit uniform, conformal films with atomic-level thickness control. Panel (a) reprinted with permission from Ref. [92]. Panel (b) reprinted with permission from Ref. [101]. Panel (c) reprinted with permission from Ref. [102]. Panel (d) reprinted with permission from Ref. [103].

3.1.1. Top-down: mechanical exfoliation and stacking

The starting point for the top-down route is the acquisition of high-quality bulk layered crystals suitable for exfoliation. These bulk crystals are typically synthesized at high temperatures using methods such as chemical vapor transport (CVT) or the flux method. The CVT method, which uses a transport agent like a halogen to grow high-quality single crystals from powder precursors under a temperature gradient, is the standard technique for obtaining most 2D magnets (like CrI_3) and TMD crystals. These synthesized, high-quality parent crystals possess a perfect layered structure and extremely weak interlayer van der Waals forces, which provide the physical prerequisite for the subsequent mechanical exfoliation process. In current laboratory research, the top-down approach of mechanical exfoliation and stacking remains the cornerstone for constructing high-quality 2D multiferroic heterostructures. This route begins with the classic Scotch-tape exfoliation method,[90] which involves repeatedly peeling bulk crystals to obtain single-crystal flakes with extremely low defect densities. This provides the most ideal source of samples for exploring intrinsic physical properties. Subsequently, researchers employ a precision technique known as dry transfer stacking, using a viscoelastic polymer stamp to pick up and stack these flakes layer-by-layer under a microscope.[91–93] By precisely controlling a rotation stage during the pickup process, the interlayer twist angle can also be set, ultimately lead-

ing to the construction of heterostructures with a specific configuration. However, the bottlenecks of this method are significant. The random nature of mechanical exfoliation leads to extremely low yield and sample sizes limited to several tens of micrometers, which severely restricts the reproducibility and scalability of research. More critically, the transfer process inevitably introduces contaminants at the interface, such as polymer residues, trapped air bubbles, and water molecules.[94,95] These atomic-scale defects severely compromise the cleanliness of the interface, introducing disorder that can completely obscure or alter the weak magnetoelectric coupling effects.

3.1.2. Bottom-up: large-area growth techniques

To overcome the size and yield limitations of the mechanical exfoliation method, bottom-up large-area growth techniques have emerged, with chemical vapor deposition (CVD)[96–98] being the most promising candidate for industrial-scale production. By reacting gaseous precursors on a catalytic substrate at high temperatures (typically 600–900 °C), CVD can grow wafer-scale 2D films and vertical heterostructures. Meanwhile, atomic layer deposition (ALD),[99,100] a variant of CVD, offers atomic-level thickness control and operates at lower growth temperatures (100–250 °C) through the use of alternating, self-limiting surface reactions, making it advantageous for stacking thermally sensitive materials. Despite their great promise, these growth techniques still face challenges in the context of multiferroic heterostructures. Compared to perfect exfoliated single crystals, CVD-grown films typically contain a higher density of grain boundaries and defects. The high-temperature environment also makes it exceedingly difficult to achieve atomically clean interfaces within the heterostructures. While ALD offers a low-temperature advantage, the crystal quality of the films it produces is often inferior, and optimizing the process to achieve high-quality crystalline growth at low temperatures remains a challenge.

3.2. Key characterization techniques

Investigating 2D multiferroic heterostructures requires characterization techniques with high sensitivity and spatial resolution to detect weak signal responses. The experimental approach typically follows a systematic progression: first confirming structural quality, then verifying the individual ferroic properties, and finally investigating the interfacial magnetoelectric coupling. This comprehensive analysis is essential for understanding the physical mechanisms governing these systems.

3.2.1. Structural and morphological characterization: the quality control of the device

Before any complex physical property measurements can be performed, the primary task is to confirm that the structure and morphology of the heterostructure meet the design specifications. Atomic force microscopy (AFM) is the most fundamental tool for this step.[104,105] By non-destructively scanning the sample surface, it can precisely measure the material thickness to determine the number of layers and check for macroscopic defects introduced during stacking, such as wrinkles and bubbles. To further probe the interface quality at the atomic scale, transmission electron microscopy (TEM) provides atomic-resolution cross-sectional imaging of the interface,[106,107] allowing for the assessment of interfacial sharpness through cross-sectional imaging and the precise determination of interlayer twist angles via electron diffraction.

3.2.2. Characterization of single ferroic orders: verifying the building blocks

After confirming the structural integrity, it is necessary to individually verify that the functional building blocks of the heterostructure — the ferroelectric and ferromagnetic layers — are each working correctly.

For the direct confirmation of ferroelectricity, piezoresponse force microscopy (PFM) is currently the core tool.[108–110] By detecting the sample's inverse piezoelectric response to an AC electric field, it not only enables direct imaging of ferroelectric domains and their polarization directions but, more importantly, can be used to switch the domains *in-situ* with DC voltage pulses and plot local piezoelectric hysteresis loops, providing evidence for the switchable nature of ferroelectricity. However, as highlighted by Gruverman *et al.*,[110] PFM signals can be obscured by non-piezoelectric artifacts arising from electrostatic forces, charge injection, and electrochemical reactions at the tip–surface junction. To rigorously distinguish intrinsic ferroelectricity, it is essential to perform switching spectroscopy PFM (SS-PFM) to verify characteristic hysteresis loops and to confirm the long-term retention of written domains to rule out transient electrostatic effects. Besides, to rigorously exclude non-ferroelectric origins, it is highly recommended to corroborate PFM results with optical second harmonic generation (SHG) measurements.[111] As a non-destructive probe sensitive to broken inversion symmetry, SHG provides definitive evidence of the polar order and its symmetry characteristics.

For the characterization of magnetism, the most common macroscopic technique is the magneto-optical Kerr effect (MOKE), which measures the net magnetization by detecting the minute rotation of polarized light upon reflection from the magnetic surface, yielding high-quality hysteresis loops.[112,113] For the direct visualization of magnetic domain distribution and evolution, researchers typically employ magnetic force microscopy (MFM).[101,114]

4. Experimental realization of magnetoelectric coupling

This section reviews pivotal experimental demonstrations of electrical control of magnetism in heterostructures. The dis-

cussion begins with hybrid-dimensional systems, which integrate 2D magnets with ferroelectric polymers or piezoelectric substrates. It then examines all-vdW heterostructures composed entirely of van der Waals crystals, where magnetoelectric coupling originates from intrinsic interfacial interactions.

4.1. Magnetoelectric coupling in hybrid-dimensional systems

Before the exploration of all-vdW multiferroic systems, researchers achieved significant early progress in hybrid-dimensional heterostructures by combining 2D magnets with well-established conventional ferroelectric/piezoelectric materials. Although these systems do not fall under the strict definition of a vdW heterostructure, they provided valuable experimental proof-of-concept for the electric-field control of 2D magnetism.

One common strategy in this area is strain-mediated magnetoelectric coupling. As shown in Figs. 8(a) and 8(b), a typical example is the work by Wang *et al.*, where a 2D vdW ferromagnet, Fe_5GeTe_2, was placed on a bulk piezoelectric single-crystal substrate, PMN-PT.[115] By applying a voltage to the PMN-PT substrate, they successfully achieved reversible and non-volatile control over the magnetization of Fe_5GeTe_2 at room temperature through the piezoelectric strain generated by the substrate. Raman spectroscopy and x-ray diffraction measurements confirmed the effective transfer of strain from the substrate to the 2D magnetic layer. This method of altering MAE via strain represents a classic and effective pathway for magnetoelectric coupling.

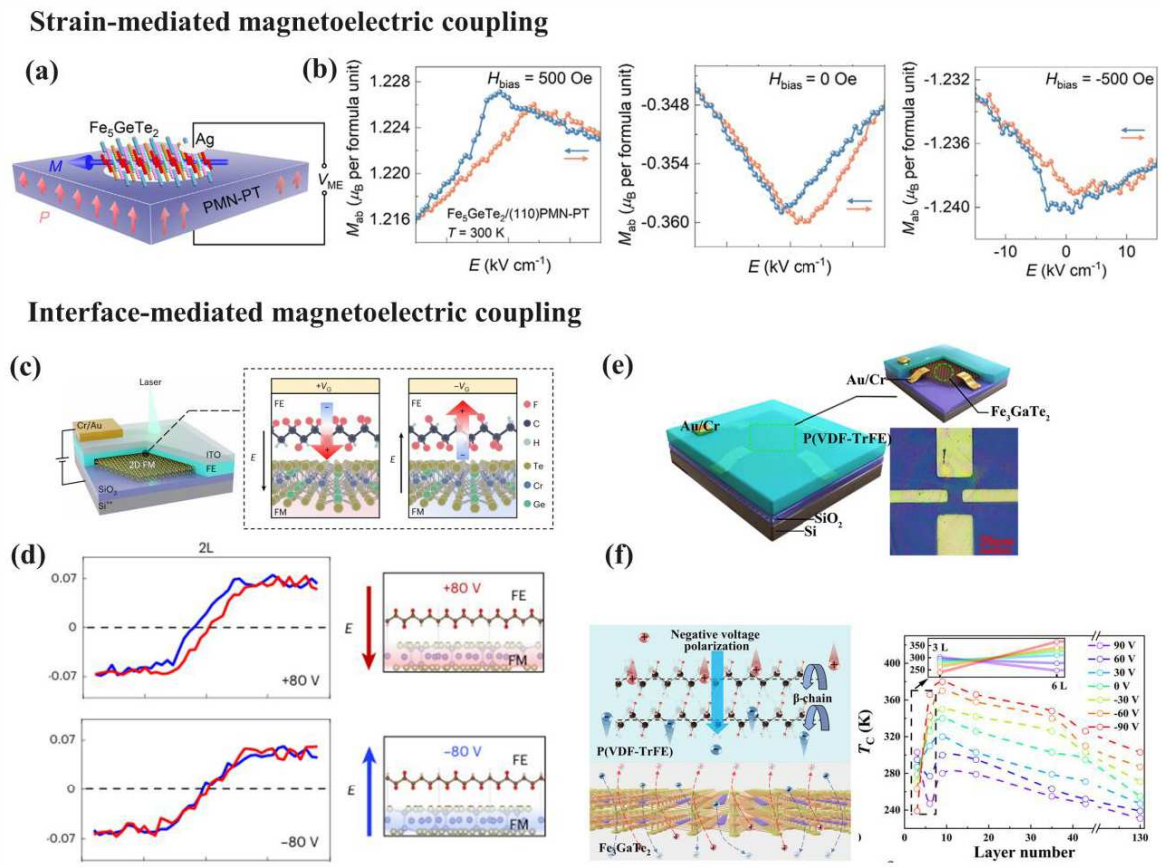


Fig. 8. Magnetoelectric coupling mechanisms in hybrid-dimensional heterostructures. (a) and (b) Strain-mediated coupling in Fe_5GeTe_2/PMN-PT. (a) Device schematic showing the 2D magnet Fe_5GeTe_2 bonded to a piezoelectric PMN-PT substrate. (b) Magnetization versus electric field curves displaying characteristic butterfly loops. This behavior indicates that piezoelectric strain transferred from the substrate modulates the magnetocrystalline anisotropy of the Fe_5GeTe_2 layer. (c) and (d) Interface-mediated switching in $Cr_2Ge_2Te_6$/P(VDF-TrFE). (c) Device structure and schematic of the atomic reconstruction at the interface induced by polarization reversal. (d) Non-volatile switching of the magnetic hysteresis loop. The structural modulation at the interface alters the magnetic anisotropy, toggling the system between a ferromagnetic state (open loop) and a paramagnetic-like state (closed loop). (e) and (f) Charge-mediated modulation in Fe_3GaTe_2/P(VDF-TrFE). (e) Device architecture. (f) Modulation of the Curie temperature (T_C) via interfacial charge accumulation or depletion. Switching the ferroelectric polarization modifies the carrier density and exchange interactions within the itinerant ferromagnet, enabling bidirectional electrical tuning of T_C. Panels (a) and (b) reprinted with permission from Ref. [115]. Panels (c) and (d) reprinted with permission from Ref. [116]. Panels (e) and (f) reprinted with permission from Ref. [117].

Another strategy that is closer to the vdW heterostructure concept involves the use of ferroelectric polymers, such as P(VDF-TrFE). Because polymer thin films can be made very thin and are flexible, they can form relatively intimate contact with 2D materials. At low temperatures (4 K), as shown in Figs. 8(c) and 8(d), Liang *et al.* combined the 2D magnetic insulator $Cr_2Ge_2Te_6$ with a ∼50 nm thick film of P(VDF-TrFE).[116] They discovered that a small voltage of

±5 V applied across the polymer could reversibly "open" and "close" the magnetic hysteresis loop of $Cr_2Ge_2Te_6$, achieving a non-volatile switching from paramagnetic-like behavior to ferromagnetic behavior. A key finding of this work was that this modulation effect was significant only in few-layer (2–4 layers) $Cr_2Ge_2Te_6$ and nearly vanished in a thicker (8-layer) sample, clearly indicating the dominant role of interfacial effects. As shown in Figs. 8(e) and 8(f), Cai *et al.* combined P(VDF-TrFE) with another room-temperature ferromagnet, Fe_3GaTe_2, and demonstrated not only non-volatile, bidirectional control of its Curie temperature at room temperature but also observed interesting layer-dependent effects.[117] These works showcase the immense potential of using flexible ferroelectrics to control 2D magnetism at the interface.

4.2. Intrinsic interfacial coupling in all-van der Waals heterostructures

Despite the significant progress in hybrid-dimensional systems, the exploration of more fundamental interface physics, as well as the construction of atomically precise all-2D devices, necessitates the study of all-vdW heterostructures composed entirely of van der Waals crystals. In such systems, the coupling no longer relies on external strain or polymers but instead originates from the intrinsic, electronic interactions across the van der Waals gap between the two crystals.

4.2.1. Proof-of-principle demonstrations at low temperatures

As shown in Figs. 9(a) and 9(b), early all-vdW multiferroic experiments were primarily focused on providing a proof of principle for the theoretically predicted interfacial coupling mechanisms at low temperatures. The heterostructure composed of the 2D antiferromagnet CrI_3 and the 2D ferroelectric α-In_2Se_3 is a canonical example. The work by Wu *et al.* utilized reflective magnetic circular dichroism (RMCD) to clearly demonstrate that the magnetic ground state of CrI_3 could be non-volatilely altered by applying a gate voltage across the α-In_2Se_3 layer.[119] The experiments revealed that the different polarization states of α-In_2Se_3 asymmetrically enhanced the interlayer ferromagnetic coupling in CrI_3, thereby achieving switching control over the interlayer magnetic exchange. This work provides direct experimental evidence for the core interfacial electronic mechanism of polarization-switched magnetic exchange. Meanwhile, Eom *et al.* also observed voltage control of the coercive field in $Fe_{3-x}GeTe_2/In_2Se_3$ heterostructures.[118] Interestingly, their evidence from Raman spectroscopy suggested that this modulation might originate more from the interfacial strain induced by the piezoelectric effect of In_2Se_3. These two works reveal the possible coexistence and competition of multiple coupling mechanisms in all-vdW heterostructures.

4.2.2. Towards room temperature: A landmark breakthrough

Bridging the gap from low temperatures to room temperature is a crucial leap for the field towards practical applications. A landmark breakthrough was recently achieved with the realization of non-volatile electrical control of magnetism at room temperature in $Fe_3GaTe_2/CuInP_2S_6$ (FGT/CIPS) heterostructures. The significance of the work by Zhao *et al.* lies in the clever selection of two van der Waals crystals that both possess room-temperature ferroic orders: the ferromagnetic metal FGT and the ferroelectric CIPS.[120]

As shown in Fig. 9(c), the researchers utilized anomalous Hall effect (AHE) measurements and found that after applying a voltage pulse sufficient to switch the polarization of the CIPS layer and then removing it, the shape of the magnetic hysteresis loop of the FGT layer was permanently and reproducibly altered, manifesting as a significant reduction in the coercive field and an evolution of the magnetic reversal mode from coherent to incoherent. *In-situ*magnetic force microscopy (MFM) confirmed that the ferroelectric polarization state directly influences the formation and pinning of magnetic domain walls. To fundamentally understand this phenomenon, the work combined first-principles calculations with micromagnetic simulations, which ultimately revealed a novel coupling mechanism: the ferroelectric polarization of CIPS induces a significant DMI at the interface and modulates the magnetic reversal behavior by controlling the strength of this DMI. This work not only achieved robust magnetoelectric control in an all-vdW system at room temperature for the first time but, more importantly, it provided a complete physical evidence chain from macroscopic transport to microscopic domains to interfacial DMI modulation. It strongly validates that ferroelectric polarization control of DMI is a novel and highly effective magnetoelectric coupling mechanism in van der Waals multiferroic heterostructures.

These pioneering experimental demonstrations, particularly the leap from low-temperature proof-of-principle to room-temperature functionality, represent a critical step for the field from scientific exploration toward technological application. The profound implications and potential applications of this electrically controlled magnetism are what drive the intense interest in the field. Now, let us turn our attention to these future technologies.

4.3. Distinguishing mechanisms via characterization

Building upon the theoretical frameworks established in Section 2, the challenge lies in experimentally pinpointing which mechanism dominates in a real device. In the experimental exploration of vdW multiferroic heterostructures, a central challenge lies in isolating the dominant magnetoelectric coupling mechanism among several coexisting possibilities. To facilitate this process, we propose a diagnostic work-

flow in Table 2, synthesizing the experimental logic from key studies detailed in Section 4.

As illustrated in the table, the distinction relies heavily on analyzing the symmetry of the response and performing structural cross-validation. For instance, charge transfer is characterized by a nonreciprocal magnetic response (dependent on the electric field polarity); however, to confirm this purely electronic mechanism, one must simultaneously rule out lattice deformation using Raman spectroscopy. In contrast, mechanisms driven by interfacial orbital hybridization typically induce a symmetric (homopolar) modulation of coercivity, which is affirmatively linked to piezoelectric strain only if voltage-dependent Raman peak shifts are observed. Finally, DMI-driven coupling is identified not merely by parameter changes, but by a fundamental evolution in the magnetic reversal mode (e.g., from coherent to incoherent), which necessitates real-space visualization (e.g., via MFM) to confirm the modulation of domain wall dynamics or skyrmion nucleation.

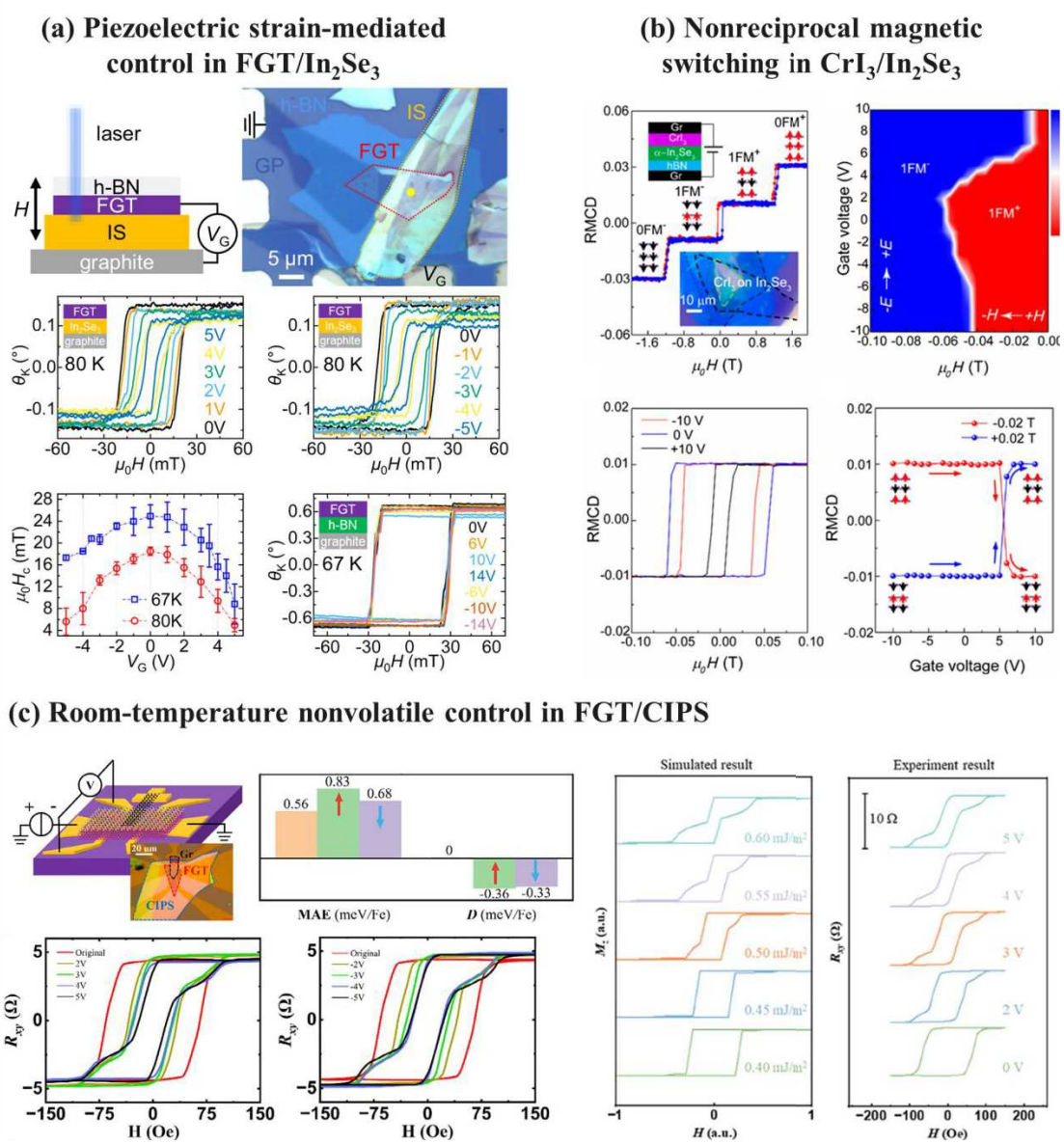


Fig. 9. Experimental realizations of electrical control of magnetism in 2D vdW multiferroic heterostructures. (a) Piezoelectric strain-mediated control in $Fe_{3-x}GeTe_2/In_2Se_3$ heterostructures. The magnetic hysteresis loops (measured by MOKE) show that the coercive field (H_c) of $Fe_{3-x}GeTe_2$ is significantly modulated by the voltage applied to the ferroelectric In_2Se_3 layer. The symmetric V-shaped H_c–V_g dependence (bottom left) and the absence of modulation in the h-BN control device (bottom right) confirm that piezoelectric strain is the dominant mechanism at low temperatures. (b) Nonreciprocal magnetic switching in CrI_3/In_2Se_3 heterostructures. RMCD measurements reveal an asymmetric shift of the spin-flip transition field under gating. This nonreciprocal behavior enables direct electrical switching between magnetic states, driven by the modulation of interlayer magnetic exchange coupling via ferroelectric polarization. (c) Room-temperature nonvolatile control in $Fe_3GaTe_2/CuInP_2S_6$ heterostructures. Anomalous Hall effect (AHE) measurements demonstrate nonvolatile modulation of magnetic hysteresis loops at room temperature. The experimental evolution of the loops with polarization voltage (right) shows excellent agreement with micromagnetic simulations (left), validating that ferroelectric polarization controls the magnetism by modulating the interfacial DMI. Panel (a) reprinted with permission from Ref. [119]. Panel (b) reprinted with permission from Ref. [118]. Panel (c) reprinted with permission from Ref. [120].

Table 2. General diagnostic criteria for identifying interfacial magnetoelectric coupling mechanisms based on experimental signatures.

Coupling mechanism	Macroscopic signal	Microscopic verification	Physical logic chain
Polarization-gated charge transfer	The magnetic state changes significantly under one electric field polarity but remains unresponsive or behaves differently under the opposite.	Raman spectroscopy shows no observable peak shifts under applied voltage, ruling out piezoelectric strain effects.	Since electrostatic doping depends on the direction of the electric field relative to the band alignment, the effect is inherently asymmetric. The lack of structural distortion confirms a purely electronic origin.
Interfacial orbital hybridization (MAE)	Key magnetic parameters decrease or increase for both positive and negative bias voltages.	Raman peaks exhibit voltage-dependent shifts that track the trend of the magnetic modulation.	The effect is driven by piezoelectric strain, which often induces similar in-plane lattice expansion regardless of polarity, thereby symmetrically modulating the orbital overlap and MAE.
Polarization-modulated DMI	Evolution of Hysteresis Loop Shape: A qualitative transition from a square loop (coherent reversal) to a slanted loop (incoherent reversal).	MFM reveals increased domain wall density or the nucleation of topological textures (e.g., skyrmions).	The change in reversal mode signals a reduction in domain wall energy, which is the direct consequence of enhanced interfacial DMI.

5. Functional characteristics and device applications

Voltage-controlled magnetism in 2D van der Waals multiferroic heterostructures presents a pathway to address the power consumption constraints of conventional electronics. Rather than examining physical effects in isolation, this section integrates these mechanisms with specific device concepts to illustrate the progression from fundamental research to potential technological applications in future information systems.

5.1. Nonvolatile magnetic memory and logic devices

The most direct application prospect for this field lies in building ultra-low-power nonvolatile magnetic memory and logic devices. Mainstream MRAM technology relies on current-driven spin-transfer torque (STT)[121] or spin–orbit torque (SOT)[122,123] to switch magnetization, a process that suffers from significant Joule heating and power consumption issues. In contrast, 2D multiferroic heterostructures provide a disruptive, voltage-controlled path to magnetism. For instance, in systems like CrI_3/α-In_2Se_3, reversing the polarization of the ferroelectric layer can directly switch the magnetic exchange between layers.[119] This state transition can be directly mapped to a high/low resistance state, enabling nonvolatile electric-write, magnetic-read memory functionality. Alternatively, leveraging ferroelectric polarization to flip the magnetic anisotropy of the magnetic layer, causing its easy axis to switch between in-plane and out-of-plane, can also alter the device's magnetoresistive state.[124] This can be used to construct voltage-tunable magnetic switches and logic gates. Such voltage-driven schemes promise to reduce the write energy by several orders of magnitude.

5.2. Brain-inspired neuromorphic computing

The multi-state and nonvolatile nature of 2D multiferroic heterostructures makes them an ideal physical platform for brain-inspired neuromorphic computing.[125,126] Conventional CMOS-based AI hardware faces enormous power and latency issues due to the von Neumann bottleneck when performing large-scale parallel computations. In a 2D multiferroic heterostructure, both the ferroelectric and magnetic layers can host multiple domains.[127–130] By applying a series of voltage pulses with controlled amplitude or width, a gradual and incomplete switching of the ferroelectric domains can be achieved. This analog change in the polarization state, in turn, modifies the overall magnetic state of the device, manifesting as a multi-level, nonvolatile change in its conductance. This process perfectly mimics the weight plasticity and long-term potentiation/depression (LTP/LTD) behavior of biological synapses, where training leads to learning, laying the foundation for energy-efficient artificial synaptic devices.

5.3. Topological and spintronic devices

Furthermore, this field presents unique opportunities for novel topological and spintronic devices. Moving beyond simple binary logic, utilizing the topological properties of matter or the spin degree of freedom of electrons to process information promises higher fault tolerance and lower energy consumption. For example, in systems like $Fe_3GaTe_2/CuInP_2S_6$,[120,131] the ferroelectric polarization, by controlling the interfacial DMI, enables the nonvolatile creation, annihilation, and even chirality reversal of magnetic skyrmions.[132–135] As topologically stable information carriers, skyrmions provide a path toward high-density, low-power racetrack memories and topological bits. On another front, theoretical predictions suggest that in certain systems (e.g., $FeCl_2/Sc_2CO_2$), the ferroelectric polarization can directly modulate the band structure of the adjacent magnetic

layer, causing a phase transition from a semiconductor to a half-metal.[136] This electric-field-induced switching of metallicity relevant to spin filtering and the realization of fully spin-polarized current sources for spin-logic,[137–139] opening new avenues for voltage-controlled spin logic operations.

5.4. Challenges for critical applications

While the device concepts discussed above demonstrate immense potential, transitioning them from laboratory prototypes to practical technologies requires overcoming specific engineering barriers. To bridge the gap between fundamental research and application, an actionable roadmap must address critical bottleneck metrics tailored to each device paradigm.

For nonvolatile memory and logic, the primary challenge lies in reliability and scalability. Although vdW interfaces theoretically minimize bonding defects, competitive devices must demonstrate fatigue resistance exceeding 10^{12} switching cycles and data retention of over 10 years at elevated temperatures. Achieving these standards necessitates a shift from exfoliation-based prototypes to wafer-scale, uniform CVD growth compatible with CMOS integration. In the field of neuromorphic computing, the focus shifts to the precision of analog switching. The key milestone here is engineering the defect landscape to ensure high linearity and symmetry in weight updates, thereby minimizing device-to-device variation that currently hinders large-scale neural network accuracy. Finally, for topological spintronics, the absolute prerequisite is thermal stability. Future efforts must prioritize identifying or engineering vdW systems — potentially via interface DMI enhancement — that can support stable skyrmion generation and manipulation at room temperature without bulky external magnetic fields.

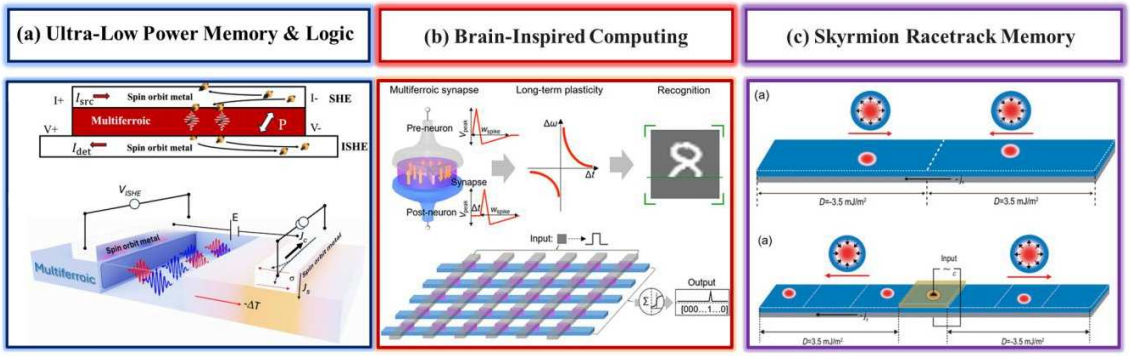


Fig. 10. Future device applications based on van der Waals multiferroic heterostructures. (a) Ultra-low power memory and logic device. This non-local architecture utilizes ferroelectric polarization to gate the generation and propagation of magnons. The signal is electrically detected via the inverse spin Hall effect, enabling voltage-controlled logic operations. (b) Brain-inspired computing. The application of voltage pulses progressively modulates the ferroelectric domain configuration, resulting in multi-level non-volatile conductance states. This analog behavior emulates the long-term plasticity of biological synapses for artificial neural networks. (c) Skyrmion racetrack memory. A conceptual single-nanotrack device where local reversal of the DMI chirality creates a barrier. This mechanism allows precise control over the creation, annihilation, and motion of skyrmions, enabling logic gate functionalities within a single nanowire. Panel (a) reprinted with permission from Ref. [140]. Panel (b) reprinted with permission from Ref. [129]. Panel (c) reprinted with permission from Ref. [141].

6. Conclusion

In summary, 2D van der Waals multiferroic heterostructures, with their unique advantages in interface quality and tunability, have emerged as a highly promising physical platform for exploring novel magnetoelectric phenomena and developing next-generation electronic devices. At the theoretical level, a rich variety of interfacial coupling mechanisms has been proposed, providing a solid physical foundation for achieving strong magnetoelectric coupling. At the experimental level, despite significant challenges, landmark breakthroughs, typified by the non-volatile electrical control of magnetism at room temperature, have successfully demonstrated the feasibility of this approach and ignited hope for disruptive applications in low-power electronics and neuromorphic computing. However, we must recognize that the path from laboratory proof of concept to mature technological application is still filled with challenges.

The current research bottlenecks can be primarily categorized into three levels: material, interface, and lifetime. First, at the material level, the construction of systems is severely limited by the scarcity of suitable materials. On one hand, many key 2D magnets (e.g., CrI_3) are chemically unstable and rapidly oxidize and degrade in ambient conditions.[42] On the other hand, the Curie temperatures of most known 2D magnets are far below room temperature, which fundamentally restricts the practical operating environment of any device.[142,143] Concurrently, the polarization strength of some 2D ferroelectrics can be considerably weaker than that of their conventional bulk counterparts.[144] Second, at the interface level, although a perfect interface is theoretically possible, actual fabrication processes, especially the dry transfer technique, inevitably introduce defects such as polymer residues, trapped bubbles, and stacking mismatch. These interfacial imperfections introduce disorder and scattering, leading to a drastic reduction in carrier mobility and can even completely obscure the faint, intrinsic magnetoelectric coupling effect that is being sought. Finally, at the device lifetime level, the fatigue effects and poor retention performance commonly found

in ferroelectric devices are also critical reliability challenges that must be addressed in these 2D systems.[145]

Despite these formidable challenges, they also clearly illuminate the directions for future research. The foremost task is undoubtedly materials discovery: accelerating the search for novel 2D ferroelectric and ferromagnetic materials that possess robust room-temperature ferroic orders, air stability, and strong coupling potential, using a combination of high-throughput computational screening and experimental synthesis. This is followed by process innovation, which involves developing contamination-free, automated, all-in-vacuum stacking techniques to overcome the current interface contamination problem, and exploring scalable direct van der Waals epitaxy methods, which are essential steps to transition from the lab to industry. Finally, in the realm of mechanism and device exploration, researchers need to delve deeper into utilizing new degrees of freedom, such as moiré superlattices, to engineer and enhance interfacial magnetoelectric coupling. It is also crucial to actively push forward from single-device physical demonstrations to the fabrication and integration of multi-pixel prototype devices, in order to ultimately transform the immense potential of 2D van der Waals multiferroic heterostructures into a tangible technology.

Acknowledgment

Project supported by the National Key R&D Program of China (Grant No. 2021YFA1202200).

References

[1] Xu X, Huang F T, Admasu A S, Kratochvílová M, Chu M W, Park J G and Cheong S W 2022 *Phys. Rev. B* **105** 184407
[2] Zimmermann A S, Meier D and Fiebig M 2014 *Nat. Commun.* **5** 4796
[3] Scott J 2007 *Nat. Mater.* **6** 256
[4] Scott J F 2013 *NPG Asia Mater.* **5** e72
[5] Martin L W and Ramesh R 2012 *Acta Mater.* **60** 2449
[6] Ahn C, Rabe K and Triscone J 2004 *Science* **303** 488
[7] Song T, Cai X, Tu M W Y, Zhang X, Huang B, Wilson N P, Seyler K L, Zhu L, Taniguchi T, Watanabe K, McGuire M A, Cobden D H, Xiao D, Yao W and Xu X 2018 *Science* **360** 1214
[8] Xuan X, Guo W and Zhang Z 2022 *Phys. Rev. Lett.* **129** 047602
[9] Xu M, Huang C, Li Y, Liu S, Zhong X, Jena P, Kan E and Wang Y 2020 *Phys. Rev. Lett.* **124** 067602
[10] Cohen R 1992 *Nature* **358** 136
[11] Ding H C and Duan C G 2012 *Europhys. Lett.* **97** 57007
[12] Miyahara S and Furukawa N 2016 *Phys. Rev. B* **93** 014445
[13] Nakajima T, Mitsuda S, Kanetsuki S, Tanaka K, Fujii K, Terada N, Soda M, Matsuura M and Hirota K 2008 *Phys. Rev. B* **77** 052401
[14] Schoenherr P, Manz S, Kuerten L, Shapovalov K, Iyama A, Kimura T, Fiebig M and Meier D 2020 *npj Quantum Mater.* **5** 86
[15] Holbein S, Steffens P, Biesenkamp S, Ollivier J, Komarek A C, Baum M and Braden M 2023 *Phys. Rev. B* **108** 104404
[16] Hill N A 2000 *J. Phys. Chem. B* **104** 6694
[17] Wang J, Fang H, Nie F, Chen Y, Tian G, Shi C, He B, Lü W and Zheng L 2022 *ACS Appl. Mater. Interfaces* **14** 48917
[18] Li H, Liao W, Sun B, Lu Y, He X, Xu Z, Huang C, Sun Z and Li T 2023 *Ceram. Int.* **49** 8325
[19] Millis A J 1997 *Phys. Rev. B* **55** 6405
[20] Mryasov O N, Sabiryanov R F, Freeman A J and Jaswal S S 1997 *Phys. Rev. B* **56** 7255
[21] Madon B, Kang H B, Kang M G, Maurya D, Magill B A, Alves M J P, Wegrowe J E, Drouhin H J, Priya S and Khodaparast G A 2018 *AIP Adv.* **8** 105034
[22] Prajapat C L, Bhatt H, Kumar Y, Rao T V C, Mishra P K, Ravikumar G, Kinane C J, Satpati B, Caruana A, Langridge S, Basu S and Singh S 2020 *ACS Appl. Electron. Mater.* **2** 2629
[23] Kumar V, Gaur A, Choudhary R J and Gupta M 2016 *J. Magn. Magn. Mater.* **405** 72
[24] Regan E C, Wang D, Paik E Y, Zeng Y, Zhang L, Zhu J, MacDonald A H, Deng H and Wang F 2022 *Nat. Rev. Mater.* **7** 778
[25] Liu J and Zhang J 2020 *Chem. Rev.* **120** 2123
[26] Kim J H, Kim S, Cho Y, Park H J, Shin H, Kwon S and Lee Z 2019 *Adv. Mater.* **31** 1807486
[27] Liu C, Yang Y, Fletcher J, Liu A, Gilley I, Iii C, Wang Z, Zhu H, Chen H, Reynolds R, Ding B, Ding Y, Zhang X, Skackauskaite R, Wan H, Zeng L, Bati A, Shibayama N, Getautis V, Chen B, Rakstys K, Dyson P, Kanatzidis M, Sargent E and Nazeeruddin M 2025 *Nat. Energy* **10** 981
[28] Zhang H, Xu T, Yu K, Wang W, He L and Sun L 2021 *Nat. Commun.* **12** 4812
[29] Guo E, Roldan M A, Charlton T, Liao Z, Zheng Q, Ambaye H, Herklotz A, Gai Z, Ward T Z, Lee H N and Fitzsimmons M R 2018 *Adv. Funct. Mater.* **28** 1800922
[30] Geim A K and Grigorieva I V 2013 *Nature* **499** 419
[31] Mirabedini P S, Debnath B, Neupane M R, Alex Greaney P, Glen Birdwell A, Ruzmetov D, Crawford K G, Shah P, Weil J and Ivanov Tony G 2020 *Appl. Phys. Lett.* **117** 121901
[32] Liu X, Cheng X and Zhang H 2022 *Phys. Lett. A* **443** 128216
[33] Xing K, McEwen D, Yin Y, Zhao W, Bake A, Cortie D, Liu J, Vu T H Y, Chen Y H, Hone J, Stacey A, Edmonds M T, Medhekar N V, Watanabe K, Taniguchi T, Ou Q, Qi D C and Fuhrer M S 2025 *ACS Nano* **19** 3579
[34] Drost R, Kezilebieke S, Ervasti M, Hämäläinen S, Schulz F, Harju A and Liljeroth P 2015 *Sci. Rep.* **5** 16741
[35] Pimenta Martins L G, Comin R, Matos M J S, Mazzoni M S C, Neves B R A and Yankowitz M 2023 *Appl. Phys. Rev.* **10** 011313
[36] Franke K and Von Oppen F 2018 *Nature* **560** 175
[37] Zheng X, Yang Y, Sun B, Ning R, Sui J and Cai W 2021 *ACS Appl. Nano Mater.* **4** 3493
[38] Bonef B, Shah R D and Mukherjee K 2019 *Nano Lett.* **19** 1428
[39] Oh S, Jung S, Ali M H, Kim J H, Kim H and Park J H 2020 *ACS Appl. Mater. Interfaces* **12** 38299
[40] Kumar A, Hameed S, Denneulin T, Balan A P, Vas J, Leutner K, Gao L, Gomonay O, Sinova J, Dunin-Borkowski R E and Kläui M 2025 *Small* **21** e06284
[41] Lüpke F, Just S, Bihlmayer G, Lanius M, Luysberg M, Dolezal J, Neumann E, Cherepanov V, Ost'ádal I, Mussler G, Grützmacher D and Voigtländer B 2017 *Phys. Rev. B* **96** 035301
[42] Zhang T, Grzeszczyk M, Li J, Yu W, Xu H, He P, Yang L, Qiu Z, Lin H, Yang H, Zeng J, Sun T, Li Z, Wu J, Lin M, Loh K P, Su C, Novoselov K S, Carvalho A, Koperski M and Lu J 2022 *J. Am. Chem. Soc.* **144** 5295
[43] Huang B, Clark G, Klein D R, MacNeill D, Navarro-Moratalla E, Seyler K L, Wilson N, McGuire M A, Cobden D H, Xiao D, Yao W, Jarillo-Herrero P and Xu X 2018 *Nat. Nanotechnol.* **13** 544
[44] Wang P, Lian F, Du R, Cai X, Bao S, Han Y, Xiao J, Watanabe K, Taniguchi T, Wen J, Yang H, Mayorov A S, Wang L and Yu G 2024 *Appl. Phys. Lett.* **124** 012406
[45] Powalla L, Birch M T, Litzius K, Wintz S, Satheesh S, Weigand M, Goering E, Schütz G and Burghard M 2023 *Phys. Rev. B* **108** 214417
[46] Deng Y, Yu Y, Song Y, Zhang J, Wang N Z, Sun Z, Yi Y, Wu Y Z, Wu S, Zhu J, Wang J, Chen X H and Zhang Y 2018 *Nature* **563** 94
[47] Boott C E, Nazemi A and Manners I 2015 *Angew. Chem. Int. Ed.* **54** 13876
[48] Chen J, Liu L, Chen H, Xu N and Deng S 2024 *ACS Appl. Mater. Interfaces* **16** 10877
[49] Wu M, Ding X, An M, Liu L, Zheng X and Hu H 2025 *ACS Appl. Nano Mater.* **8** 12653
[50] Lu Y, Wang H, Xu X, Wang L and Yang L 2025 *Phys. Rev. B* **111** 165410
[51] Xu X and Yang L 2025 *Nano Lett.* **25** 1050
[52] Gao Y, Zhou B and Wang X 2021 *Phys. Chem. Chem. Phys.* **23** 6171
[53] Deus D P D A, Lopes J M J and Miwa R H 2023 *Carbon* **213** 118244
[54] Yuan L, Zheng B, Kunstmann J, Brumme T, Kuc A B, Ma C, Deng S, Blach D, Pan A and Huang L 2020 *Nat. Mater.* **19** 617

[55] Tong L, Peng Z, Lin R, Li Z, Wang Y, Huang X, Xue K H, Xu H, Liu F, Xia H, Wang P, Xu M, Xiong W, Hu W, Xu J, Zhang X, Ye L and Miao X 2021 *Science* **373** 1353

[56] Bobkov G A, Bokai K A, Otrokov M M, Bobkov A M and Bobkova I V 2024 *Phys. Rev. Mater.* **8** 104801

[57] Dong P, Hou X, He J, Zhang Y, Ding Y, Zeng X, Wang J, Wu Y, Watanabe K, Taniguchi T, Xia W, Guo Y, Chen Y, Zhou X, Li W and Li J 2024 *Phys. Rev. B* **109** L140503

[58] Bistritzer R and MacDonald A H 2011 *Proc. Natl. Acad. Sci. USA* **108** 12233

[59] Cao Y, Fatemi V, Fang S, Watanabe K, Taniguchi T, Kaxiras E and Jarillo-Herrero P 2018 *Nature* **556** 43

[60] Cao Y, Fatemi V, Demir A, Fang S, Tomarken S L, Luo J Y, Sanchez-Yamagishi J D, Watanabe K, Taniguchi T, Kaxiras E, Ashoori R C and Jarillo-Herrero P 2018 *Nature* **556** 80

[61] Tang Y, Li L, Li T, Xu Y, Liu S, Barmak K, Watanabe K, Taniguchi T, MacDonald A H, Shan J and Mak K F 2020 *Nature* **579** 353

[62] Rivera P, Yu H, Seyler K L, Wilson N P, Yao W and Xu X 2018 *Nat. Nanotechnol.* **13** 1004

[63] Fei Z, Zhao W, Palomaki T A, Sun B, Miller M K, Zhao Z, Yan J, Xu X and Cobden D H 2018 *Nature* **560** 336

[64] Wang H, Chen Z and Peng B 2025 *Sci. China Mater.* **68** 928

[65] Wang L, Wang X, Zhang Y, Li R, Ma T, Leng K, Chen Z, Abdelwahab I and Loh K P 2020 *Adv. Funct. Mater.* **30** 2004609

[66] Cui C, Hu W J, Yan X, Addiego C, Gao W, Wang Y, Wang Z, Li L, Cheng Y, Li P, Zhang X, Alshareef H N, Wu T, Zhu W, Pan X and Li L J 2018 *Nano Lett.* **18** 1253

[67] Jiang X, Wang Z, Li C, Sun X, Yang L, Li D, Cui B and Liu D 2024 *Chin. Phys. Lett.* **41** 057501

[68] Panday S R, Barraza-Lopez S, Rangel T and Fregoso B M 2019 *Phys. Rev. B* **100** 195305

[69] Yin G, Guo Y, Ke Y, Zhang L, Zhang J and Quhe R 2023 *Physica E* **154** 115814

[70] Chen R, Meng F, Zhang H, Liu Y, Yan S, Xu X, Zhu L, Chen J, Zhou T, Zhou J, Yang F, Ci P, Huang X, Chen X, Zhang T, Cai Y, Dong K, Liu Y, Watanabe K, Taniguchi T, Lin C C, Penumatcha A V, Young I, Chan E, Wu J, Yang L, Ramesh R and Yao J 2025 *Nat. Commun.* **16** 3648

[71] Li L and Wu M 2017 *ACS Nano* **11** 6382

[72] Ding J, Xiang H, Zhou W, Liu N, Chen Q, Fang X, Wang K, Wu L, Watanabe K, Taniguchi T, Xin N and Xu S 2024 *Nat. Commun.* **15** 9087

[73] Behera P, Ross A M, Shanker N, Meisenheimer P, Manna M, Lin C, Hsu S, Harris I, Kavle P, Husain S, Ojha S K, Das S, Raja A, Martin L W, Susarla S, Salahuddin S, Chen L and Ramesh R 2025 *Adv. Mater.* **37** 2410149

[74] Mermin N D and Wagner H 1966 *Phys. Rev. Lett.* **17** 1133

[75] Yin L, Berlijn T, Juneja R, Lindsay L and Parker D S 2022 *Phys. Rev. B* **106** 085117

[76] Tong W Y, Gong S J, Wan X and Duan C G 2016 *Nat. Commun.* **7** 13612

[77] Du Q, Wang W, Tang F, Su W, Wu J, Hu Z, Wang Z and Liu M 2024 *ACS Appl. Mater. Interfaces* **16** 7463

[78] De Assis I R, Mertig I and Göbel B 2023 *Phys. Rev. B* **108** 144438

[79] Gong C, Li L, Li Z, Ji H, Stern A, Xia Y, Cao T, Bao W, Wang C, Wang Y, Qiu Z Q, Cava R J, Louie S G, Xia J and Zhang X 2017 *Nature* **546** 265

[80] Huang B, Clark G, Navarro-Moratalla E, Klein D R, Cheng R, Seyler K L, Zhong D, Schmidgall E, McGuire M A, Cobden D H, Yao W, Xiao D, Jarillo-Herrero P and Xu X 2017 *Nature* **546** 270

[81] Zhao Y, Zhang J, Yuan S and Chen Z 2019 *Adv. Funct. Mater.* **29** 1901420

[82] Lu Y, Fei R, Lu X, Zhu L, Wang L and Yang L 2020 *ACS Appl. Mater. Interfaces* **12** 6243

[83] Yu X, Zhang X and Wang J 2023 *ACS Nano* **17** 25348

[84] Gong C, Kim E M, Wang Y, Lee G and Zhang X 2019 *Nat. Commun.* **10** 2657

[85] Hur J H 2021 *Phys. Chem. Chem. Phys.* **23** 25925

[86] Sun W, Wang W, Li H, Zhang G, Chen D, Wang J and Cheng Z 2020 *Nat. Commun.* **11** 5930

[87] Chen J, Gui C and Dong S 2024 *Phys. Rev. B* **110** L060406

[88] Huang K, Shao D F and Tsymbal E Y 2022 *Nano Lett.* **22** 3349

[89] Sun R J, Liu R, Lu J J, Zhao X W, Hu G C, Yuan X B and Ren J F 2022 *Phys. Rev. B* **105** 235416

[90] Novoselov K S, Geim A K, Morozov S V, Jiang D, Zhang Y, Dubonos S V, Grigorieva I V and Firsov A A 2004 *Science* **306** 666

[91] Dean C R, Young A F, Meric I, Lee C, Wang L, Sorgenfrei S, Watanabe K, Taniguchi T, Kim P, Shepard K L and Hone J 2010 *Nat. Nanotechnol.* **5** 722

[92] Castellanos-Gomez A, Buscema M, Molenaar R, Singh V, Janssen L, Van Der Zant H S J and Steele G A 2014 *2D Mater.* **1** 011002

[93] Wang L, Meric I, Huang P Y, Gao Q, Gao Y, Tran H, Taniguchi T, Watanabe K, Campos L M, Muller D A, Guo J, Kim P, Hone J, Shepard K L and Dean C R 2013 *Science* **342** 614

[94] Yang F, Liu J, Lu Z, Dai P, Nakamura T, Wang S, Chen L, Wakamiya A and Matsuda K 2020 *Adv. Sci.* **7** 1902474

[95] Rizu M I, Fadil D and Llobet E 2025 *npj 2D Mater. Appl.* **9** 28

[96] Hoque M, George A, Ramachandra V, Najafidehaghani E, Gan Z, Mitra R, Zhao B, Sahoo S, Abrahamsson M, Liang Q, Wiktor J, Turchanin A, Kubatkin S, Lara-Avila S and Dash S 2024 *npj 2D Mater. Appl.* **8** 55

[97] Shin W, Byeon J, Koo R H, Lim J, Kang J H, Jang A R, Lee J H, Kim J J, Cha S, Pak S and Lee S T 2024 *Adv. Sci.* **11** 2307196

[98] Hoque A, Ramachandra V, George A, Najafidehaghani E, Gan Z, Mitra R, Zhao B, Khokhriakov D, Turchanin A, Lara-Avila S, Kubatkin S and Dash S P 2023 *Phys. Rev. Mater.* **7** 044005

[99] Kim C, Hur N, Yang J, Oh S, Yeo J, Jeong H Y, Shong B and Suh J 2023 *ACS Nano* **17** 15776

[100] Zhu R, Zhao R, Gao K, Zhang Z, He Q, Tong H and Miao X 2024 *Adv. Funct. Mater.* **34** 2408897

[101] Ni Y, Guo Y, Jiang Y, Huang T, Mu Q, Hou F, Li T, Wang S, Zhang Z, Shao D, Ding X, Min T and Li T 2025 *Small* **21** 2409189

[102] Wang S, Wang X and Warner J H 2015 *ACS Nano* **9** 5246

[103] Kim H G and Lee H B R 2017 *Chem. Mater.* **29** 3809

[104] Gao Y, Weston A, Enaldiev V, Li X, Wang W, Nunn J E, Soltero I, Castanon E G, Carl A, De Latour H, Summerfield A, Hamer M, Howarth J, Clark N, Wilson N R, Kretinin A V, Fal'ko V I and Gorbachev R 2024 *Nat. Commun.* **15** 4449

[105] Li Y, Yang Y, Zhao H, Duan H, Yang C, Min T and Li T 2025 *Nano Lett.* **25** 1680

[106] Kelly D J, Clark N, Zhou M, Gebauer D, Gorbachev R V and Haigh S J 2021 *Adv. Mater.* **33** 2100668

[107] Ni Y, Wang T, Wang J, Guo Y, Huang T, Qiao X, Zhang W, Zhang Z, Chen X, Li T and Min T 2024 *Adv. Phys. Res.* **3** 2300116

[108] Li T, Wu Y, Yu G, Li S, Ren Y, Liu Y, Liu J, Feng H, Deng Y, Chen M, Zhang Z and Min T 2024 *Nat. Commun.* **15** 2653

[109] Zhou Y, Yang C, Fu X, Liu Y, Yang Y, Wu Y, Ge C, Min T, Zeng K and Li T 2024 *ACS Appl. Mater. Interfaces* **16** 13247

[110] Gruverman A, Alexe M and Meier D 2019 *Nat. Commun.* **10** 1661

[111] Abdelwahab I, Tilmann B, Wu Y, Giovanni D, Verzhbitskiy I, Zhu M, Berté R, Xuan F, Menezes L S, Eda G, Sum T C, Quek S Y, Maier S A and Loh K P 2022 *Nat. Photonics* **16** 644

[112] Yao W, Li Y, Yang M, Hou F, Li T and Min T 2024 *J. Magn. Magn. Mater.* **611** 172599

[113] Gibertini M, Koperski M, Morpurgo A F and Novoselov K S 2019 *Nat. Nanotechnol.* **14** 408

[114] Niu Y, Liu Z, Wang K, Ai W, Gong T, Liu T, Bi L, Zhang G, Deng L and Peng B 2024 *Adv. Mater.* **36** 2403066

[115] Wang Q, Yan J, Gao X, Yu Z, Yue D, Mu C, Cheng Y, Nie A, Xue T, Liu L and Zhai K 2025 *Small* **21** e10429

[116] Liang S, Xie T, Blumenschein N A, Zhou T, Ersevim T, Song Z, Liang J, Susner M A, Conner B S, Gong S J, Wang J P, Ouyang M, Žutić I, Friedman A L, Zhang X and Gong C 2023 *Nat. Electron.* **6** 199

[117] Cai C, Wen Y, Yin L, Cheng R, Wang H, Feng X, Liu L, Jiang C and He J 2025 *Nat. Commun.* **16** 6797

[118] Eom J, Lee I H, Kee J Y, Cho M, Seo J, Suh H, Choi H J, Sim Y, Chen S, Chang H J, Baek S H, Petrovic C, Ryu H, Jang C, Kim Y D, Yang C H, Seong M J, Lee J H, Park S Y and Choi J W 2023 *Nat. Commun.* **14** 5605

[119] Wu Y, Zhang D, Zhang Y N, Deng L and Peng B 2024 *Nano Lett.* **24** 5929

[120] Zhao H, Yang C, Liu Y, Wang Q, Wu Y, Mu Q, Hou F, Min T and Li T 2025 *Adv. Mater.* **37** 2500534

[121] Vincent A F, Larroque J, Locatelli N, Ben Romdhane N, Bichler O, Gamrat C, Zhao W S, Klein J O, Galdin-Retailleau S and Querlioz D 2015 *IEEE Trans. Biomed. Circuits Syst.* **9** 166

[122] Dieny B and Chshiev M 2017 *Rev. Mod. Phys.* **89** 025008

[123] Loh K P 2025 *Sci. China Mater.* **68** 1303

[124] Yang R, Zhang X, Xiao J, Yan Z, Wang F and Xu X 2025 *Chin. Phys. Lett.* **42** 070705

[125] Yang J, Wang R, Ren Y, Mao J, Wang Z, Zhou Y and Han S 2020 *Adv. Mater.* **32** 2003610

[126] Wang Z, Wu H, Burr G W, Hwang C S, Wang K L, Xia Q and Yang J J 2020 *Nat. Rev. Mater.* **5** 173

[127] Li D L, Zhong W M, Tang X G, He Q, Jiang Y P and Liu Q X 2024 *Appl. Phys. Lett.* **124** 253501

[128] Dou S, Yang X, Yuan J, Xia Y, Bai X, Cui H and Wei B 2023 *IEEE Magn. Lett.* **14** 1

[129] Yang Y, Xi Z, Dong Y, Zheng C, Hu H, Li X, Jiang Z, Lu W C, Wu D and Wen Z 2020 *ACS Appl. Mater. Interfaces* **12** 56300

[130] Sun Y, Lin T, Lei N, Chen X, Kang W, Zhao Z, Wei D, Chen C, Pang S, Hu L, Yang L, Dong E, Zhao L, Liu L, Yuan Z, Ullrich A, Back C H, Zhang J, Pan D, Zhao J, Feng M, Fert A and Zhao W 2023 *Nat. Commun.* **14** 3434

[131] Hu Q F, Huang Y Q, Wang Y, Ding S J, Zhang M J, Hua C Q, Li L J, Xu X F, Yang J B, Yuan S J, Watanabe K, Taniguchi T, Lu Y H, Jin C H, Wang D W and Zheng Y 2024 *Nat. Commun.* **15** 3029

[132] Zhou F, Shaikh M, Sun W, Chen F, Chen X, Li S, Tong H, Sanyal B and Wang D 2024 *npj 2D Mater. Appl.* **8** 51

[133] Chen Z, Hu H, Wu X, Zhang W, Li P and Song C 2025 *Phys. Rev. B* **111** 144418

[134] Acharya K, Huang K, Tsymbal E Y and Paudel T R 2025 *Phys. Rev. B* **111** 094435

[135] Wang Z, Xue F, Qiu L, Wang Z, Wu R and Hou Y 2024 *Nano Lett.* **24** 4117

[136] Cao L, Deng X, Zhou G, Liang S J, Nguyen C V, Ang L K and Ang Y S 2022 *Phys. Rev. B* **105** 165302

[137] Qiu L, An Y, Shang L, Li Y, Gong C, Chu J, Hu Z and Gong S J 2025 *J. Alloys Compd.* **1027** 180578

[138] Zhang X, Liu B, Huang J, Cao X, Zhang Y and Guo Z X 2024 *Phys. Rev. B* **109** 205105

[139] Datta S and Das B 1990 *Appl. Phys. Lett.* **56** 665

[140] Husain S and Ramesh R 2025 *npj Spintron.* **3** 36

[141] Yu D, Yang H, Chshiev M and Fert A 2022 *Natl. Sci. Rev.* **9** nwac021

[142] Che G, Gao B and Xu Q 2025 *2D Mater.* **12** 015008

[143] Huang H, Zhao Y, Zhang Z, Wang L, Wu Y, Liu C, Zhao J, Qiao G, Zhang J, Zheng X, Zhou S and Wang S 2024 *APL Mater.* **12** 041107

[144] Zheng C, Yu L, Zhu L, Collins J L, Kim D, Lou Y, Xu C, Li M, Wei Z, Zhang Y, Edmonds M T, Li S, Seidel J, Zhu Y, Liu J Z, Tang W X and Fuhrer M S 2018 *Sci. Adv.* **4** eaar7720

[145] Park S, Lee D, Kang J, Choi H and Park J H 2023 *Nat. Commun.* **14** 6778